Connexin Type and Fluorescent Protein Fusion Tag Determine Structural Stability of Gap Junction Plaques*[S]

Randy F. Stout, Jr.[‡], **Erik Lee Snapp**[§], and **David C. Spray**[‡1]

From the ‡*Dominick P. Purpura Department of Neuroscience and the* §*Department of Anatomy and Structural Biology, Albert Einstein College of Medicine, Bronx, New York 10461*

Background: Connexin proteins form gap junction channel clusters termed plaques.
Results: Microscopy with fluorescent protein-tagged connexins showed that connexin26 and connexin30 plaque arrangement is dynamic, but gap junctions of connexin43 are stabilized by its C-terminal region.
Conclusion: The arrangement of channels in gap junctions depends on connexin type.
Significance: These findings help to clarify how gap junction plaque dynamics and composition could modulate intercellular communication.

Gap junctions (GJs) are made up of plaques of laterally clustered intercellular channels and the membranes in which the channels are embedded. Arrangement of channels within a plaque determines subcellular distribution of connexin binding partners and sites of intercellular signaling. Here, we report the discovery that some connexin types form plaque structures with strikingly different degrees of fluidity in the arrangement of the GJ channel subcomponents of the GJ plaque. We uncovered this property of GJs by applying fluorescence recovery after photobleaching to GJs formed from connexins fused with fluorescent protein tags. We found that connexin 26 (Cx26) and Cx30 GJs readily diffuse within the plaque structures, whereas Cx43 GJs remain persistently immobile for more than 2 min after bleaching. The cytoplasmic C terminus of Cx43 was required for stability of Cx43 plaque arrangement. We provide evidence that these qualitative differences in GJ arrangement stability reflect endogenous characteristics, with the caveat that the sizes of the GJs examined were necessarily large for these measurements. We also uncovered an unrecognized effect of non-monomerized fluorescent protein on the dynamically arranged GJs and the organization of plaques composed of multiple connexin types. Together, these findings redefine our understanding of the GJ plaque structure and should be considered in future studies using fluorescent protein tags to probe dynamics of highly ordered protein complexes.

Gap junction (GJ)[2] plaques are made up of dodecameric protein channels embedded in the plasma membranes of adjacent cells. GJ channels form direct pathways for intercellular communication and are important for development and function of most tissues in the human body, including the brain. GJ channels are composed of connexin subunits. Six connexin transmembrane proteins interact with connexin hexamers on adjacent membranes to form an individual GJ channel spanning two membranes and thereby connecting cytoplasmic compartments. GJ channels cluster into very densely packed and organized two-dimensional arrays that take on a paracrystalline arrangement. These clusters of many individual GJ channels are termed gap junction plaques. The advent of green fluorescent proteins and derivatives for use as fusion proteins (1–3) allowed observation of the live characteristics of connexins within the GJ plaque structure. The results of initial pioneering studies have yielded some hard to reconcile results. For example, some live imaging studies have indicated that GJs can have extremely static arrangements over the course of hours (approximating the lifetime of the proteins within the structure), whereas other studies have indicated a large amount of rearrangement of channels within the plaques (4–8). Even in situations where very static plaque arrangement was observed, "global" plaque shape changes were observed over a short time scale (6) (*i.e.* large sections of the plaque can split or fuse without major rearrangement of individual GJ channels relative to the position of neighboring channels). We wondered how local order is maintained during large scale plaque morphology changes and have used new fluorescent proteins and fast live confocal microscopy to provide insights into GJ plaque structural dynamics.

Gap Junction Plaque Organization

Connexin subunits are assembled into hexameric connexons (half-GJs) in the endoplasmic reticulum or the Golgi apparatus, depending on connexin type (9–11). Upon traffic to the membrane (12), connexons diffuse in the plane of the membrane and when encountering appositional connexons can dock via interactions of extracellular loops. This docking process occurs in parallel with the clustering of the newly formed GJ channels into an orthogonal array with positioning constrained by the cellular membranes of the two junctional cells. Molecular mechanisms underlying this important cellular process are not well understood.

Almost all cells express multiple connexin genes. Connexins can come together to form mixed type GJs, either heterotypic, with connexons of one type pairing with connexons of another, or heteromeric, where connexons are heterogeneous with respect to connexin composition (see Ref. 13). Beginning with the earliest groundbreaking imaging studies of exogenously expressed connexins tagged with different wavelength-emitting fluorescent proteins, it has been thought that connexins of different gene classes (α type, such as $\alpha1$ Cx43, and β type, such as $\beta2$ Cx26 or $\beta6$ Cx30) are restricted to segregated pools within the same GJ plaque (6, 14–17). GJ channel characteristics and non-channel-based cellular functions vary by connexin type. Posttranslational modifications to connexins can be spatially arranged into specific patterns within the GJ plaque and modulate intercellular communication (18, 19).

GJ plaque arrangement stability and steady-state structure are both potentially important to cellular function and intercellular communication. Therefore, we reexamined these issues. We focus on connexins co-expressed in mammalian astrocytes using new generation fluorescent protein tags optimized with respect to correct folding and lack of dimerization. Imprecise terminology for fluorescence recovery after photobleaching (FRAP) studies of GJ biology has led to confusion when comparing results from different studies. The persistence of GJ plaques at the membrane (often referred to as "gap junction stability") and the movement of whole plaque structures in the membrane ("plaque mobility") describe macro-behavior of GJs. We examine the stability of the arrangement of the GJ channels within the GJ plaque ("plaque arrangement stability") of astrocyte-expressed connexins Cx43, Cx30, and Cx26.

Experimental Procedures

Cell Culture and Transfection—HeLa cells were plated into 8-well imaging chambers (ibidi, LCC), and each well was transfected with 0.5 μg of each plasmid to drive expression of connexin-fluorescent protein fusions 24–72 h before imaging. Optifect (Life Technologies, Inc.) was used to transfect the plasmids according to the manufacturer's instructions adjusted for the surface area of the wells of the ibidi chambers (50 μl of Opti-MEM medium and 3 μl of Optifect reagent per well). Opti-MEM medium was replaced with the standard growth medium for HeLa and N2A cells (DMEM with 10% fetal bovine serum and 1% penicillin-streptomycin) or the standard growth medium of RINm cells (RPMI1640 medium with 10% fetal bovine serum and 1% penicillin-streptomycin) 12–16 h after transfection. Cells were incubated in standard growth medium for at least 6 h before imaging.

Plasmids and Subcloning—The coding sequence for Cx43, Cx30, and Cx26 were inserted in-frame into plasmids based on the Clontech EGFP-N1 and EGFP-C1 backbone. Plasmids used for this study contain the CMV promoter with a short linker between an N- or C-terminal superfolder GFP (sfGFP), enhanced blue fluorescent protein 2 (EBFP2), or monomerized Venus (mVenus) tags (20, 21). Monomeric sfGFP (msfGFP) contains a V206K monomerizing mutation (22–24). sfGFP (25) contains a valine residue encoded at position 206 in the fluorescent protein sequence, and GFP derivatives (*e.g.* EGFP, enhanced cyan fluorescent protein, and enhanced yellow fluorescent protein) with an alanine or valine at this position have a weak tendency to dimerize (22–24). Cx26 and Cx43 coding sequences used for fluorescent protein fusion constructs were from rats. All Cx30 constructs were made with the human GJB6 coding sequence. Untagged Cx26 and Cx43 expression constructs for immunostaining were from mouse Gjb2 and Gja1 coding sequence, respectively. Rodent and human connexin protein sequences are highly homologous within connexin type (*e.g.* human and rat Cx43 and Cx30 protein sequences are 97 and 95% identical, respectively). The linker sequence for N1 plasmids (those constructs with the FP tag on the C terminus (CT) of the connexin) containing rat Cx26 is ADPPVAT, that for N1 plasmids containing human Cx30 is YPDPPVAT, and that for N1 plasmids containing rat Cx43 is SADPPVAT. The linker is SGLRSRAQ for all C1 plasmids (constructs with the FP tag on the amino terminus of the connexin). Plasmids were sequenced from both ends of the coding region for overlapping sequence verification. The Cx43K258stop truncation was made using PCR cloning with the InFusionHD kit. Rat Cx43 with a stop codon inserted at position 258 (and the rest of the CT omitted) was inserted into the multiple cloning site of sfGFP-C1 and EBFP2-C1 plasmids. The Cx43K258stop sequence was transferred to sfGFP-N1 and msfGFP-N1 plasmids, in frame with the fluorescent protein and with the stop codon removed. This plasmid construction was performed with the InFusionHD PCR cloning kit. The truncation constructs used the same linker sequence as the full-length Cx43 constructs. Plasmids used for this study are available at the Addgene online repository.

Microscopy and FRAP—15–30 min before imaging, medium was removed and replaced with imaging medium (26) containing 10% fetal bovine serum, 25 mM HEPES, and 2 mM glutamine in DMEM without phenol red. The ibidi imaging chambers were then placed in the incubator for 10–15 min before transport to the confocal microscope, where they were kept in a chamber maintained at 37 °C on the stage of a Zeiss LSM 510 Live with Duo module and imaged with a ×63, numerical aperture 1.4 oil immersion objective. The detector consists of dual 512-pixel linear arrays of CCD camera-type pixels. Pixel size was 200 nm for FRAP experiments and 100 nm for three-dimensional *Z*-stacks. Cells were imaged at 500-ms intervals with 405-nm (EBFP2), 489-nm (GFP variants, mVenus, and Alexa Fluor 488), and 561-nm (Alexa Fluor 594) laser illumination for both image acquisition and bleaching. For general FRAP experiments, the bleach region was set to bleach 2 μm of the GJ plaque aligned on end, which in single z-plane time lapse acquisitions forms a line that is, in practical terms, limited to one

dimension by the resolution limit of standard light microscopy. Bleaching for FRAP with an 80/20 splitter in place and laser power set to 100% was performed on membrane 2×4-μm rectangle regions at a scan speed of 5 frames/s and three iterations for GFP and five iterations for EBFP2. A serial Z-section through the cells was conducted before each FRAP experiment. Each FRAP experiment consisted of 20 prebleach acquisitions followed by bleaching of the region of interest, which was followed by 220 single plane scans at 500-ms intervals. Immediately following the final single-plane acquisition of the FRAP experiment, a second Z-section was performed as close to 2 min after the bleach time point as possible. Due to the high sensitivity of microscope detectors and high signal intensity from the sfGFP fluorophores on each GJ (12 per GJ channel), the laser power required for postbleach time lapse acquisitions was exceptionally low, resulting in minimal acquisition photobleaching.

Heteromeric Gap Junction FRAP—HeLa and N2A cells were co-transfected with plasmids. For heteromeric GJ experiments with untagged connexins, the tagged and untagged connexin plasmids were premixed at a ratio of 1:4 with 500 ng of the plasmid encoding fluorescent protein-tagged connexin and 2 μg of the plasmid encoding the untagged plasmid. The same imaging and bleaching settings were used for heteromeric FRAP as were used for all tagged connexin FRAP experiments except that an additional higher intensity Z-stack was acquired before and after the FRAP experiment because the heteromeric plaques were variable in intensity but generally at least 50% dimmer than GJs made up of purely tagged connexins.

Heterotypic Gap Junction FRAP—Cells were transfected in separate culture dishes with different plasmids. 12 h after transfection, the cells were washed once in growth medium and twice in PBS, and then one of the dishes of cells was trypsinized and replated into the container of the other cells with the other transfection. One group of cells was transfected with sfGFP-tagged connexin in the wells of the 8-well ibidi chambered slide. Each well of the slide received 1 μg of DNA. The other group was transfected in a 3.5-cm culture dish with 4 μg of DNA for plasmids containing untagged Cx43 (CMV promoter-driven mouse Cx26 and EF1α promoter-driven rat Cx43 and rat Cx43S257stop). Cells sourced from the dish transfected with untagged connexin were marked in the following ways. N2A cells were loaded with CellTracker Orange CMTMR (Thermo Fisher, catalog no. C2927) 12 h after the transfection and before replating into the ibidi 8-well chambered slide. The HeLa cells were from a line stably expressing CMV promoter-driven mCherry (cytoplasmic localized). The resulting cultures contained both homotypic GJs (tagged::tagged, untagged::untagged) and heterotypic GJs (tagged::untagged). The heterotypic GJs were identified first by their lower fluorescence and shape of Cx-msfGFP localization (half of the cell pair without expression). The heterotypic GJs were then confirmed by the presence of orange dye (N2A cells) or mCherry (HeLa cells) in one of the two cells, the cell not expressing Cx-msfGFP. FRAP was performed with the same imaging and bleaching settings as were used for other FRAP experiments.

Immunostaining—HeLa cells grown in 8-well ibidi dishes were transfected 48 h before immunostaining with combinations of Cx43, Cx26, Cx26-msfGFP, msfGFP-Cx26, sfGFP-Cx26, and/or Cx26-sfGFP. 12 h after the transfection mixture was applied (Optifect + DNA + Opti-MEM medium), the Opti-MEM medium was replaced with DMEM with 10% FBS and penicillin/streptomycin. Cells were allowed to grow for 24 h and then were washed two times with PBS and then fixed for 20 min in 4% paraformaldehyde in PBS at room temperature. Cells were washed three times in PBS and then incubated in blocking solution (4% goat serum and 0.1% Triton X-100 in PBS) for 1 h. Cells were then washed twice with PBS, and then primary antibody was applied. Cells expressing untagged Cx43 were stained with rabbit polyclonal antibody against Cx43 CT, 1:500 (C6219, Sigma), for 16 h at 4 °C. Cells expressing untagged Cx43 and Cx26 were stained with mouse anti-Cx26 antibody (30-8100, Invitrogen) in addition to the same Cx43 antibody and in the same conditions as above. Cells were then washed six times in PBS and then stained with Alexa Fluor594-labeled donkey anti-rabbit secondary antibody (1:1000) for 1 h at room temperature (Alexa Fluor488-labeled goat anti-mouse secondary antibody was included for staining Cx43 and Cx26). Cells were then washed six times in PBS and imaged using the Zeiss 5Live microscope with a $\times$63 PlanApo numerical aperture 1.4 oil objective.

FRAP Analysis—To generate recovery curves, the bleach region was outlined as the region of interest (ROI), and the fluorescent protein pool was defined as the entire plaque within the focal plane (Fig. 1). Recovery curves were generated by correcting for loss of signal due to bleach and for acquisition-bleach of the total pool of fluorescent protein and normalized to 100% prebleach and 0% for the initial postbleach time point to normalize for incomplete bleaching within the bleach ROI as described previously (27). Background values were subtracted from both the bleach ROI and the fluorescence pool ROI. A correction factor was calculated by dividing the average of the 10 fluorescence pool readings preceding the bleach (initial fluorescence of the fluorescence pool; $fpFo$) by the fluorescent pool ROI readings at each time point (Fp), ($fpFo/Fp$). The bleach ROI reading (bF) for each time point was divided by the bleach region baseline-initial fluorescence Fo (bFo) (bF/bFo), and the resulting fraction of initial fluorescence was then multiplied by the correction factor. The resulting corrected fractional fluorescence was then multiplied by 100% to calculate "normalized recovery (%)." With the omission of background subtraction, transforming to complete bleach baseline, and averaging to generate initial fluorescence pool values, the calculations for the recovery curve values were as follows. Normalized percent FRAP values at each time point were calculated with the following equation.

$$\%FRAP = (\,fpFo/Fp) \times (bF/bFo) \times 100\% \qquad \text{(Eq. 1)}$$

Correction for loss of signal due to bleach was necessary because the 2-μm linear bleach area eliminated a substantial portion of the total fluorescence pool (average 43 ± 15, 38 ± 15, and $48 \pm 14\%$ for Cx43-, Cx30-, and Cx26-msfGFP, respectively, shown in Fig. 1). The 2-μm linear bleach size was chosen
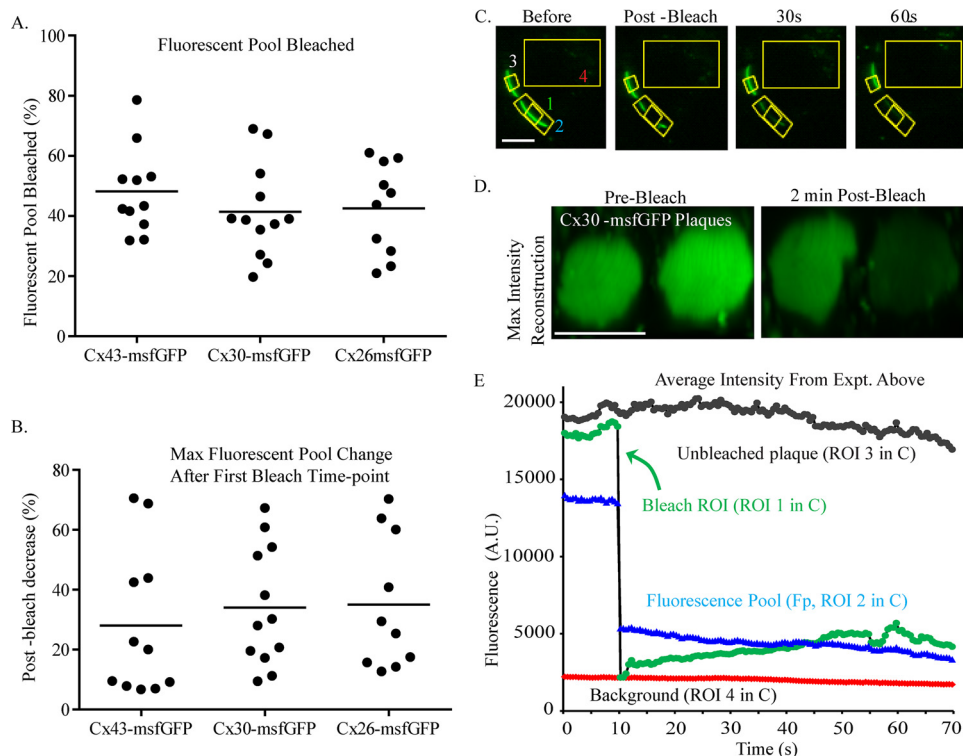
FIGURE 1. **Characterization of FRAP experiments on GJ plaques.** *A*, the percentage of the fluorescence pool that is bleached (fraction of the plaque within the two-dimensional confocal plane bleached) is larger than is standard for FRAP experiments on membrane proteins. This is due to several factors. 1) A plaque is effectively a one-dimensional structure, although the majority of the fluorescence pool is out of the focal plane. 2) The plaque size (true fluorescence pool available for recovery on the time scale of <2 min) is variable. 3) Any tilt in the plaque orientation away from parallel to the light path will alter the shape of the intersection of the bleaching laser with the plaque in out of focus regions of the plaque. 4) Reduction of the size of the bleach region below 2 μm would lead to drastically increased error due to cell shape changes (whole plaque movement); this form of error has an intrinsic bias toward recovery because any movement of the plaque will lead to less thoroughly bleached areas of the plaque moving into the focal plane. *B*, maximum percentage change in fluorescence pool average intensity (normalized to postbleach fluorescent pool intensity) over 60 s was not significantly different for the Cx-msfGFP groups. This indicates that whole plaque movement and the combined effect of out-of-focus bleach and arrangement fluidity were, altogether, not significantly different. No significant difference was seen in any groups in these figures as analyzed by ANOVA followed by Tukey's multiple comparison test. *C*, time lapse images of a Cx30-msfGFP-expressing cell pair in which two separate plaques were formed side by side. ROIs were created around the region of the plaque to be bleached (*ROI 1*), around the plaque to be bleached (*ROI 2*; fluorescence pool), around the plaque that did not have any part bleached (*ROI 3*), and a part of the cell without GJ plaque (*ROI 4*; background). *White scale bar*, 5 μm. *D*, three-dimensional reconstructions of the plaques in *C*. *Left*, prebleach; *right*, 2 min postbleach; the plaque that was bleached is less bright all over because bleached Cx43-msfGFP has redistributed throughout the plaque area. The plaque on the *left* changes shape, but overall brightness changes very little during the FRAP experiment in *C*. *White scale bar*, 2 μm. *E*, non-normalized traces showing the average fluorescence intensities for each of the ROIs in *C*. *Green*, ROI 1 (bleach region); the bleach event creates a step down in intensity at 10 s. The relatively minor apparent recovery is due to a large percentage of the fluorescence pool being bleached. Normalization corrects this error in FRAP curves. *Blue*, ROI 2, fluorescence pool. The step down (*gray*, ROI 3, unbleached plaque; little change over 1 min) indicates minor acquisition bleach. *Red*, ROI 4, background. Minimal change in background is observed. *A.U.*, arbitrary units.

because it was small enough to minimize the percentage of the plaque that was bleached while large enough to help minimize the effect of cell and plaque movement, which can cause significant systematic error in FRAP experiments performed on GJ plaques. The normalized data points at 30 s after the bleach time point were used in comparison with the percent recovery at 30 s.

Comparison of post-FRAP three-dimensional reconstructions with FRAP recovery curves and percent recovery indicated that these measures do not provide absolutely reliable quantitation of stability of the plaque structure due to particular aspects of the GJ plaque, such as shape changes and whole plaque movement. Therefore, we performed an alternative analysis to minimize errors generated by variable plaque size, out of focus bleaching, and whole plaque movement. We refer to our approach in this study as "bleach border analysis" to differentiate it from other methods to assess protein dynamics using FRAP. Bleach border analysis examines the rate at which the sharp border between bleached and unbleached regions of

the plaque (created by photobleaching of an ROI within the plaque) transitions to a diffuse blurred gradient due to rearrangement of plaque components (Fig. 2). The sharpest point in the border between bleached and unbleached sections of the plaque was identified by the peak of the absolute value of the differential of a line scan along the plaque. A border bleach value is calculated at immediately postbleach (0 s) and at 30 s postphotobleach, as described in the legend to Fig. 2. The ratio of the border sharpness at the two time points (0 s postbleach peak border)/(30 s postbleach peak border) is calculated for each FRAP experiment and then normalized to the 0 s postbleach peak border and expressed as a percentage.

The procedure for calculation of bleach border analysis was as follows. FIJI/ImageJ software (28, 29) was used to rotate the plaque to a horizontal position, and then the average intensity of each pixel for five horizontally stacked 20-pixel-wide line scans was extracted for the first postbleach image and the first image 30 s after the photobleach event, as shown in Fig. 2, *A* and *D*. The line scan intensity data were transferred to IGOR PRO
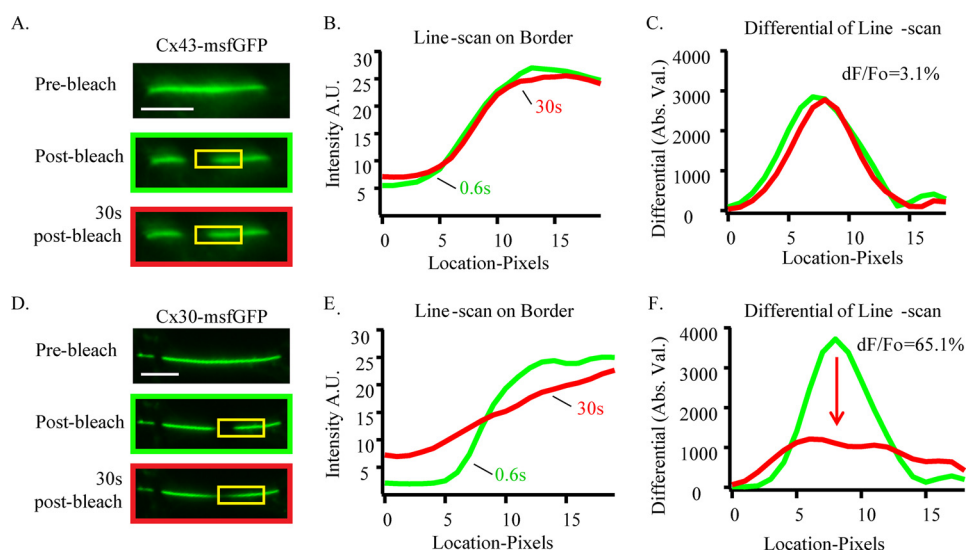
FIGURE 2. **Examples of border analysis for Cx43-msfGFP (*A–C*) and Cx30-msfGFP (*D–F*).** *A* and *D*, time lapse image of a Cx-msfGFP plaque prebleach, 0.6 s postbleach, and 30 s postbleach. *Yellow box*, region used for a 5-pixel high (5× averaged line scan) and 20-pixel-wide analysis. *Scale bar*, 5 μm. Pixel size = 0.2 μm. *B* and *E*, 5× averaged line scan across the bleach border smoothed 3×. *C* and *F*, absolute value of the differential at each point along the curves from *B* and *E*. The maximum value for 30 s postbleach was subtracted from the maximum value from 0.6 s postbleach, and this value was normalized by dividing it by the 0.6 s postbleach maximum to obtain change (*dF*) of the initial value (*Fo*), and this fraction was expressed as a percentage. This operation was performed on the image data from each FRAP experiment used in bleach border analysis, and the *dF/Fo*% (percent border blur at 30 s) was expressed as mean ± S.E. in Figs. 3–8. *A.U.*, arbitrary units.

version 6.36 (Wavemetrics) software, where it was smoothed 3× by nearest neighbor smoothing. Example smoothed line scan plots are shown in Fig. 2, *B* and *E*. The absolute value of the differential of the smoothed curve at each data point was calculated as plotted in Fig. 2, *C* and *F*. The IGOR Pro package "Multipeak Fitting 2" was used to locate the peak value of the differential and that peak value at 0 s postbleach and 30 s postbleach was compared between groups. This procedure provides a measure of the sharpness of the bright-to-dark bleach-generated border and allows for some plaque movement in the *x* and *y* directions of the image sample because locating the peak of the change from light to dark effectively localizes the center of the bleach border, even if the plaque and the bleach border within it move slightly. Bleach border analysis, however, does not correct for plaque movement in the axis of the light path.

Comparison of Average Plaque Intensity and FRAP for Heterotypic and Heteromeric Gap Junctions—Intensity data for six of the brightest pixels (assessed visually) within the plaque from the single plane acquisition of the FRAP experiment at the time point before photobleaching were exported using the ROI manager-measure function in the ImageJ/FIJI software. The measurements were exported to Microsoft Excel, and the six points were averaged. The per plaque average intensity was then compared by averaging by group for heterotypic (tagged::untagged) GJ analysis. Student's two-tailed *t* tests were used to test for significant differences between tagged::untagged (heterotypically tagged) and tagged::tagged (homotypically tagged) plaque brightness with $p < 0.05$ considered a significant difference. Individual plaque-average intensity was compared with the normalized percent recovery at 30 s postbleach for heteromeric (tagged/untagged) GJ plaques. Pearson correlation was used to test whether there was correlation between heteromeric plaque brightness and percent recovery at 30 s postbleach.

Comparison of Gap Junction Intraplaque Mixing and Three-dimensional Reconstructions—A three-dimensional reconstruction was generated as a maximum projection reconstruction in Imaris software (Bitplane). Serial *Z*-sections were spaced 0.44 or 0.25 μm apart. An orthoslicer channel was applied to the three-dimensional reconstruction in Imaris software and aligned by hand before export as a tiff file. The striping or moiré pattern that is present in three-dimensional reconstructions is an artifact of the three-dimensional reconstruction processing in conjunction with the thickness of the plaque in one dimension in comparison with the other two spatial directions (see supplemental Movie 1). Image cropping and size adjustments were performed in Adobe Illustrator CS4 software. To measure the average length of mixed GJ plaques, the images were examined as three-dimensional maximum projection reconstructions in Zen2.1 Lite Black edition (Carl Zeiss) to visually assess whether plaques with both connexins present were intermingling or segregated by channel type. GJs were considered to be non-mixed if both connexin types were observed at the continuous structure and if there were areas within the structure that had subregions that favored one color channel over the other. To measure average plaque size, the same image *Z*-stack was loaded into FIJI (29) ImageJ1.48q (28). A line was drawn across the length of the GJ plaque, and the measure function was used to measure the length of each plaque in the *xy* plane at which the plaque was widest.

Production of Supplemental Movies—All supplemental movies were prepared in Zen Lite (version 2012 black edition; Carl Zeiss) and/or Imaris (Bitplane) software and then assembled, cropped, and captioned in Corel Video Studio Pro X4 (Corel Corp.). Images were acquired on a Zeiss 5Live Duoscan microscope with a ×63 PlanApoFluor numerical aperture 1.4 oil immersion objective. Reconstructions from three-dimensional

Z-stack acquisitions for supplemental Movies 1–4 were generated in ZenLite 2012 software set to reconstruct with maximum precision and no thresholding. Reconstructions were generated by rotation around the *y* axis at 5° steps. Example FRAP experiments in supplemental Movies 1–4 are shown at 10× speed and re-encoded at 30 frames/s and assembled with three-dimensional reconstructions using Corel Video Studio Pro X4 (FRAP movies remain at 10× speed, 120 s in real experimental time is shown, and duration of FRAP experiment as displayed in movies is 12 s). Three-dimensional FRAP movies were generated from three-dimensional reconstructions in ZenLite2012 software from three-dimensional *Z*-stack time lapse acquisitions. The image interval is listed within the movie (a 3–5-s interval). These movies were re-encoded at 30 frames/s and captioned in Corel Video Studio Pro X4. Dual-color three-dimensional reconstructions for supplemental Movies 7–11 were generated using Imaris software as in Figs. 8–10 with key-frame manual rotation and on/off switching of individual color channels to show GJ plaque structure. Supplemental Movies 7–11 were re-encoded at 30 frames/s in Corel Video Studio Pro X4.

Statistics—Comparisons between data groups were performed as stated in each figure legend and as relevant throughout using GraphPad Prism version 6. $p < 0.05$ was considered a significant difference between groups. Groups were compared using one-way ANOVA followed by Tukey's multiple comparison test unless otherwise noted.

Results

Mobility of Gap Junction Channels within Plaques—We used FRAP of msfGFP-tagged connexins (msfGFP attached to the CT of the connexin protein by a short linker) to test the mobility of GJ channels. We did not compare diffusion of single proteins or multimers in relation to the cell or the coverslip. Instead, we used FRAP to test for rearrangement of proteins within GJ plaques. Movement of the entire plaque structure and cell shape changes can occlude differences in intraplaque arrangement stability. Additionally, the highly variable size and geometric arrangement of GJ plaques make standard methods of assessing diffusion coefficient and mobile fraction through analysis of single *z*-plane time lapse FRAP experiments infeasible for this work (30). GJ plaques are very anisotropic structures that can vary in size from less than 100 nm to 20 μm. Our results and those of others (4–8) indicate that the majority of recovery after photobleach within a GJ plaque comes only from channels making up the plaque at the bleach time point. This means that the fluorescence pool available for recovery is only the GJs making up the plaque when considered on a time scale of less than 5 min. We performed FRAP experiments on plaques ranging from 4–30 μm for this study, but because our bleach size was 2 μm, this led to bleaching of ~7–50% of the total fluorescence pool and up to 80% of the fluorescence pool when only the part of the plaque visible within the single confocal plane is considered (Fig. 1*A*). These challenges to analysis of the mobile fraction and calculation of the effective diffusion coefficient become more severe due to systematic differences in plaque size and geometry for the groups to be compared (Cx43, Cx30, and Cx26). Because gap junction plaques vary in size, the percentage of fluorescence pool eliminated with a constant 2-μm

bleach size was variable, leading to substantial variability in apparent percent recovery (Fig. 1*A*). Movement of the entire gap junction plaque within the cell led to variability in the *apparent* fluorescence pool, as detected in single-plane confocal acquisitions over time during the postbleach acquisition period (Fig. 1*B*). Together, these sources of variation led to increased error bars in measures of FRAP. Moreover, the three-dimensional curved and anisotropic geometry of plaques requires custom FRAP analysis techniques.

Given these complicating issues for the standard use of the FRAP technique, we focused our analysis on identifying factors that control the rate of rearrangement of the GJ channels that make up the plaque structure. Therefore, we compare three parameters of how rapidly the GJ channels change their position within the plaque (plaque arrangement instability). 1) For cursory comparison of plaque arrangement stability, we present the recovery of average fluorescence signal within the bleached region over time and compare percent recovery at a single, early time point (30 s postbleach). 2) Because plaque size and geometry vary widely from cell to cell within the same treatment group, we also compare rearrangement with a more focused assay; we compared the rate of blurring of the bleach border (a bleached/unbleached border forms when GFP on a subsection of the plaque is photobleached). 3) We performed three-dimensional reconstructions 2 min after photobleaching in order to avoid the effects of whole plaque movement or cell shape change.

Cx26 and Cx30 Are Mobile, but Cx43 Is Not—We found that Cx26 (Cx26-msfGFP) and Cx30 (Cx30-msfGFP) GJs rapidly rearrange within the plaque, whereas Cx43 (Cx43-msfGFP) GJs did not show detectable positional rearrangement during 2 min of postbleach observation in any part of the plaque structure (Fig. 3 and supplemental Movies 2–6). No detectable rearrangement (blurring of the bleach border) was observed for Cx43 in longer term observation (up to 1 h; Fig. 3*D*). This behavior was reflected in much greater recovery of fluorescence for Cx26-msfGFP and Cx30-msfGFP in the photobleached region over the course of 2 min than for Cx43-msfGFP, as shown in time lapse imaging and by normalized FRAP curves for average intensity for the bleach region over the course of 60 s (Fig. 3, *A–E*). The percent normalized FRAP at 30 s was significantly higher for Cx26-msGFP and Cx30-msfGFP (Fig. 3*F*). A small but non-zero recovery for Cx43-msfGFP was obtained when FRAP was analyzed as normalized percent recovery at 30 s. This differed from the total absence of recovery seen with analysis of bleach-border blurring (Fig. 3*F*) or three-dimensional reconstructions of the bleached plaque 2 min after photobleach (Fig. 3*D* and supplemental Movies 2 and 4). We observed that a very sharp border was created by the photobleaching event on Cx43-msfGFP plaques, and it was maintained for at least 2 min thereafter. Rearrangement of the photobleached Cx43 was never observed in three-dimensional reconstructions acquired up to 1 h postbleach (Fig. 3*D*). Given these results, we conclude that there is no rearrangement of Cx43 channels within the plaque in our experimental conditions and that the small apparent recovery in normalized average fluorescence of the bleach ROI was the result of plaque movement during the imaging experiment. These results are in
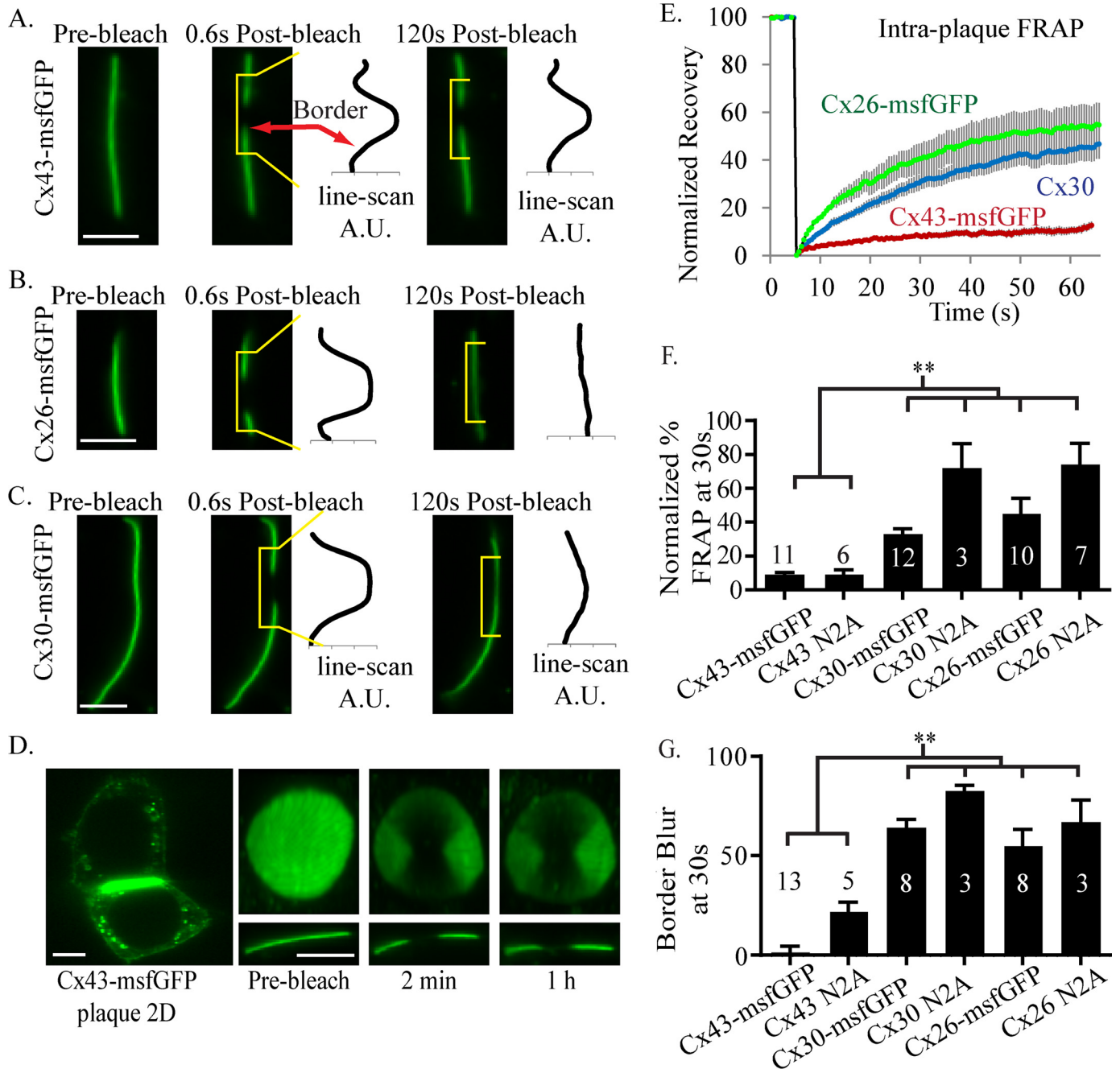
FIGURE 3. **GJ plaque arrangement dynamics depend on connexin type.** *A–C*, single plane confocal time lapse images showing, from *left* to *right*, prebleach, 0.6 s after photobleach, and 2 min after photobleach. A line scan (from the area of the GJ plaque indicated by the *yellow bracket*) shows the intensity profile of the bleach region to illustrate recovery or lack thereof. *A*, Cx43-msfGFP GJs do not rearrange their respective positions within the plaque, as indicated by the maintenance of a sharp bleach border (steep transition in intensity at edge of bleach) at 2 min. *B*, Cx26-msfGFP GJ plaques are very dynamically arranged, as indicated by significant movement of unbleached Cx26-msfGFP into the bleach region and blurring of the bleach border. *C*, Cx30-msfGFP plaques are also dynamically arranged. *D*, Cx43-msfGFP GJ arrangement is static for >1 h. *Left*, single-plane confocal image of a pair of HeLa cells joined by a plaque aligned with the axis of the light path. *Right panels*, *top row* shows a maximum projection reconstruction of the plaque at each time point with a single plane image shown *below*. *E*, normalized percent recovery (%FRAP) over time for each connexin shown in *A–C*. n = 11,10, 12, for Cx43, Cx26, and Cx30, respectively. *F*, recovery (percent normalized recovery of fluorescence into the bleach region) of Cx43 is significantly less than both Cx26 and Cx30 (in both HeLa cells and N2A cells) as analyzed by ANOVA followed by Tukey's multiple comparison test. *G*, bleach border blurring for Cx43 is significantly less than both Cx26 and Cx30 as analyzed by ANOVA followed by Tukey's multiple comparison test. **, $p < 0.01$. Numbers of GJs analyzed are shown *beside* the *bars* in bar graphs. *Error bars*, S.E. *Scale bars* (*A–D*), 5 μm. *A.U.*, arbitrary units.

agreement with previous reports indicating that a sharp border between bleached and unbleached tags marking Cx43 location can be maintained >1 h after photobleach (6). These findings highlight the extreme difference in mobility behavior between Cx43 compared with Cx30 and Cx26. A difference in mobility

between Cx43 and Cx26 was reported previously (5), but our new data indicate that the difference is substantial. We replicated these findings (Fig. 3*E*) in connexin-deficient N2A (transformed neural origin mouse cells) and RINm cells (Table 3) in order to rule out a cell line-specific effect and because HeLa

cells sometimes express a very small number of Cx45 channels endogenously, resulting in channel activity detectable only by dual-cell patch clamp electrophysiological recordings (31). These core results are summarized in Table 1. The striking and reproducible differences in plaque arrangement stability that we found led us to further characterize the arrangement of GJs within the plaque and to identify mechanisms underlying such differences.
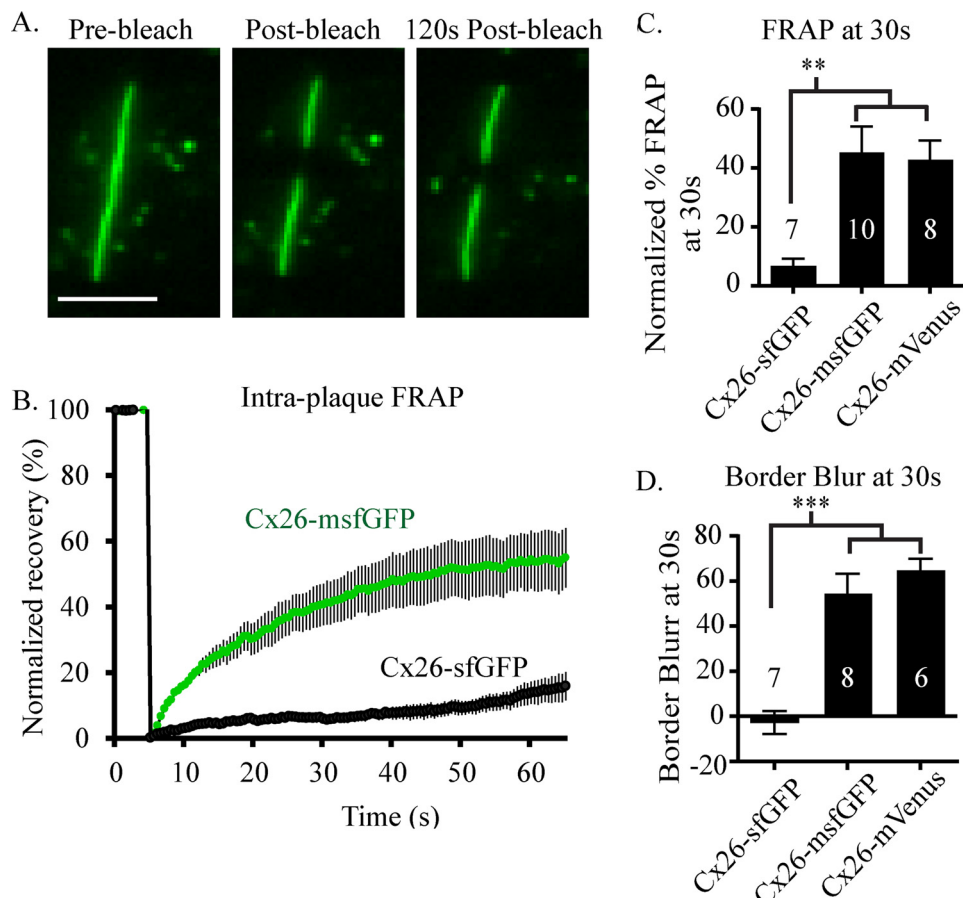
Effects of Fluorescent Protein Tags on Mobility—Previous studies on GJ mobility, trafficking, and plaque structure have used a variety of fluorescent proteins as new generation tags have been developed. Oligomerization of fluorescent protein tags has long been a concern (32), and sensitive new methods

indicate that sfGFP shows an increased tendency to aggregate/oligomerize compared with sfGFP with a V206K monomerizing mutation (msfGFP) (22, 33). When we tested for an effect of sfGFP on plaque arrangement stability, we found that Cx30 and Cx26 tagged with sfGFP had different mobility characteristics than connexins tagged with msfGFP (Fig. 4). The connexin and linker sequences were identical, with the only difference being in residue 206 of the fluorescent protein tag. Rearrangement of Cx26-sfGFP and Cx30-sfGFP was significantly less than that of Cx26-msfGFP and Cx30-msfGFP at 30 s postbleach as analyzed by comparison of percent normalized recovery (Fig. 4, *A–C*) and by border analysis at 30 s postbleach (Fig. 4*D*).

The N terminus of connexin proteins is expected to be tucked into the pore of the channel based on x-ray crystallography on Cx26 and other studies (34, 35). Attachment of a fluorescent protein fusion tag to the N terminus (NT) of connexins has been found to eliminate channel activity, but the plaques formed by the NT-tagged connexins appear similar to those formed by CT-tagged connexins and to those observed in immunostaining for untagged connexins overexpressed in HeLa cells (4). Relocation of the fluorescent protein tag would be expected to reposition the tag from the lateral edge of the

TABLE 1
Summary of main FRAP results

Connexin and Tag	Expected topology at GJ plaques	Stable or Fluid channel arrangement	Figure	Cell types tested
Cx26-msfGFP		Fluid	Fig. 3	HeLa, N2A, RINm
Cx30-msfGFP		Fluid	Fig. 3	HeLa, N2A
Cx43-msfGFP		Stable	Fig. 3	HeLa, N2A,
Cx43K258stop-msfGFP		Fluid	Fig. 6	HeLa, N2A,

FIGURE 4. **Fluorescent protein tag dimerization blocks mobility of otherwise dynamically arranged Cx26.** *A*, Cx26-sfGFP plaque arrangement is static. Single plane confocal images before, 0.6 s after, and 2 min after photobleach. *Scale bar*, 5 μm. *B*, averaged normalized recovery for Cx26-msfGFP (*top trace*, sourced from Fig. 3) and Cx26-sfGFP. For Cx26-sfGFP and Cx26-msfGFP, $n = 7$ and 10, respectively. *C*, Cx26 tagged with non-monomerized sfGFP has significantly less recovery at 30 s (average percent recovery) compared with Cx26-msfGFP and Cx26-mVenus (mVenus has a monomerizing lysine at position 206). *D*, border analysis also indicates a significant reduction in plaque arrangement fluidity at 30 s postbleach for Cx26 tagged with original sfGFP compared with Cx26-msfGFP and Cx26-mVenus. *Error bars*, S.E. Data for Cx26-msfGFP are sourced from Fig. 3. Groups were compared by ANOVA followed by Tukey's multiple comparison test. The number of experiments is listed on each *bar* of the graphs. **, $p < 0.01$; ***, $p < 0.001$. Non-monomerized fluorescent protein tag has a similar effect on Cx30 but does not affect Cx43.
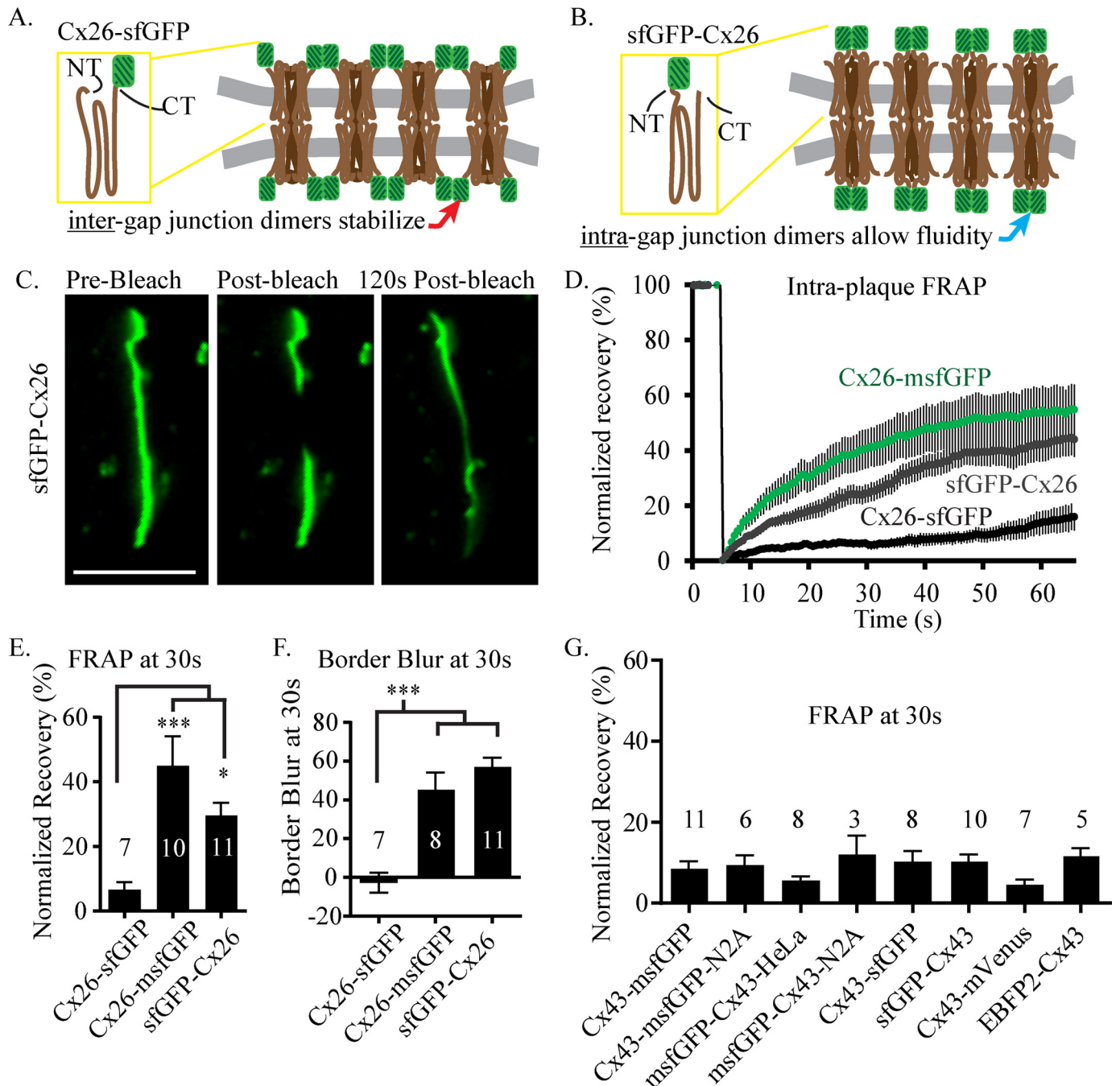
FIGURE 5. **Translocation of original sfGFP from the CT of Cx26 to the NT occludes the stabilizing effect of tag dimerization.** *A*, illustration of a single Cx26 protein (*brown*) tagged with sfGFP on the CT on the *left* and a *side view* illustration of a small plaque with GJs spanning the membranes (*gray lines*) of adjacent cells. Note that the fusion of GFP to the CT of the connexin positions it near the outside of the channel (within the cytoplasm of the cells), which may allow it to dimerize with GFP attached to a neighboring different channel. *B*, illustration showing that when the GFP is attached to the NT of the Cx26, it is probably positioned more closely to the channel pore and away from neighboring channels. *C*, plaques made up of sfGFP-Cx26 are not stably arranged. Single plane confocal images prebleach, 0.6 s postbleach, and 2 min postbleach. *D*, averaged normalized recovery for Cx26-msfGFP (*green top trace*, sourced from Fig. 3), Cx26-sfGFP (*black/green bottom trace*, sourced from Fig. 4), and sfGFP-Cx26 (*blue*, $n = 13$). *E*, Cx26 tagged with non-monomerized sfGFP on the NT has significantly more recovery at 30 s (average percent recovery) compared with Cx26-sfGFP; there was no significant difference between sfGFP-Cx26 and Cx26-msfGFP. *F*, border analysis also indicates that the bleach-induced border blurs significantly more when the sfGFP is attached to the NT than when it is on the CT, at 30 s postbleach. *G*, Cx43 forms stably arranged GJ plaques regardless of tag type and tag location. *Error bars*, S.E. Groups were compared by ANOVA followed by Tukey's multiple comparison test. The number of experiments per group is indicated *above* the bar graph for each group. *, $p < 0.05$; ***, $p < 0.001$. Cx43 plaque arrangement stability is not affected by non-monomerized fluorescent protein tag. Some data for *G* are sourced from Fig. 3.

cytoplasmic part of the GJ channels to the medial part of the channels as illustrated in Fig. 5, *A* and *B*. Furthermore, in a previous report in which Simek *et al.* (4) used a different form of FRAP analysis, the authors noted an increased percentage of plaques with highly mobile connexins when the non-mono-

merized fluorescent protein tag was changed from the CT of Cx43 to the NT. We compared FRAP for Cx26, Cx30, and Cx43 tagged on the NT (msfGFP-Cx26, sfGFP-Cx26, msfGFP-Cx30, sfGFP-Cx30, msfGFP-Cx43, and sfGFP-Cx43) as shown in Fig. 5, *D–F*. We found that both msfGFP-Cx26 and sfGFP-Cx26

were more mobile than Cx26-sfGFP. Together, these results further support the hypothesis that the stability observed for Cx26-sfGFP is due to interactions between fluorescent protein tags and are summarized in Table 2. The significantly higher mobility for sfGFP-Cx26 compared with Cx26-sfGFP (Fig. 5,

TABLE 2
Additional FRAP results- effects of protein tag and tag location

| Connexin and Tag	Expected topology at GJ plaques	Stable or Fluid channel arrangement	Figure	Cell types tested
Cx26-sfGFP		Stable	Fig. 4	HeLa
sfGFP-Cx26		Fluid	Fig. 5	HeLa
Cx30-sfGFP		Stable	Fig. 4	HeLa
sfGFP-Cx30		Fluid	Fig. 5	HeLa
sfGFP-Cx43		Stable	Fig. 5	HeLa, N2A, RINm[a]
msfGFP-Cx43		Stable	Fig. 5	HeLa
Cx43K258stop-sfGFP		Stable	Fig. 6E	HeLa, N2A
sfGFP-Cx43K258stop		Fluid	Fig. 6E	HeLa, N2A

[a] Recovery was never observed in FRAP experiments with RINm cells expressing sfGFP-Cx43 with average percent normalized recovery of $9.3 \pm 4.7\%$ at 30 s postbleach in seven experiments, this small apparent recovery in single plane FRAP experiments was an artifact of whole plaque movement since no recovery was ever observed when three-dimensional reconstructions acquired 2 min postbleach were examined.

C–F) indicates that the placement of the fluorescent protein tag at the NT of the connexin protein can occlude the effect of fluorescent protein tag aggregation on connexin mobility. However, there was no difference in plaque arrangement stability between Cx43-msfGFP (Fig. 3) and msfGFP-Cx43, sfGFP-Cx43, EBFP2-Cx43, and Cx43-mVenus (Fig. 5G, and as assessed by three-dimensional reconstruction of Z-stacks after FRAP). These results indicate that some aspect of the Cx43 protein (other than aggregation of the fluorescent protein tag) is responsible for the observed stability of GJ arrangement for this connexin.

The C Terminus of Cx43 Is Required for Plaque Arrangement Stability—The CT of Cx43 contains binding sites for many proteins that could act as a scaffold to stabilize the GJ plaque. A previous study by another group using FRAP and non-mono-merized GFP tags noted a modest increase in the percentage of plaques with >15% recovery (the fraction of mobile protein was used as a measure of total percent recovery in the study by Simek *et al.* (4)) when the CT of Cx43 was removed by truncation at amino acid 244. It is important to note that these experiments were performed with Cx43 truncated at amino acid 244 but with a non-monomerized CT GFP tag on the connexin. We performed FRAP experiments with Cx43 that we mutated to remove most of the CT by truncation. Cx43K258stop-msfGFP and sfGFP-Cx43K258stop formed very fluidly arranged GJ plaques (Fig. 6). Cx43K258stop is shown as Cx43t258 in the
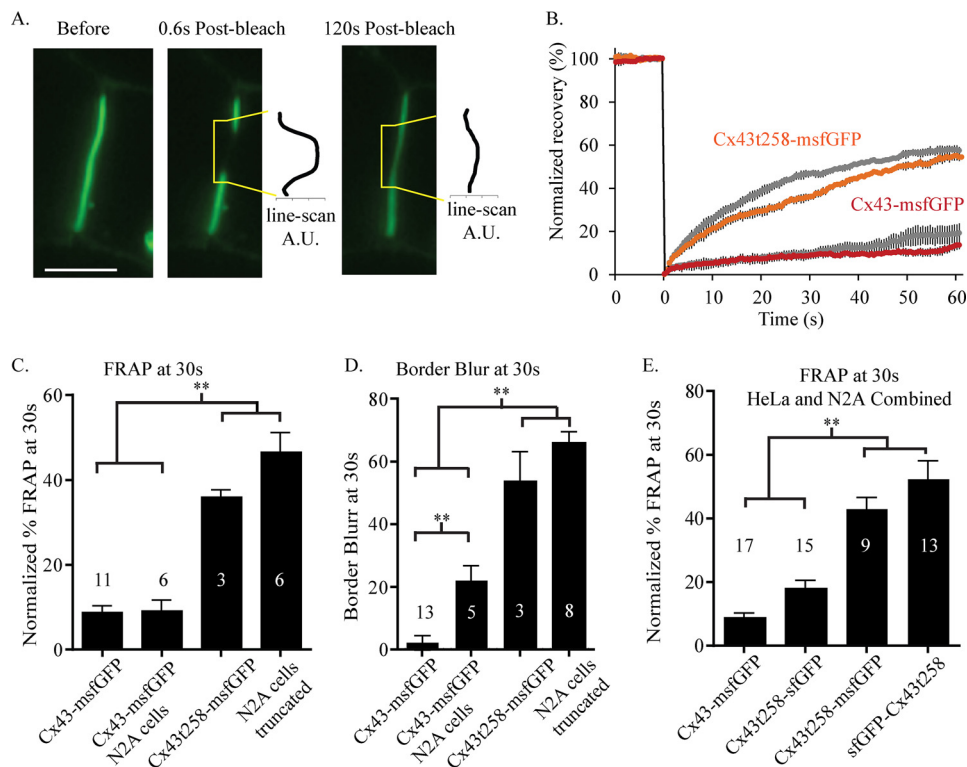
FIGURE 6. **Cx43 plaque arrangement stability requires the cytoplasmic CT.** *A*, Cx43 truncated at amino acid 258 forms GJ plaques (*left*). GJ plaques made up of Cx43K258stop-msfGFP are fluidly arranged as indicated by movement of unbleached fluorescent protein-tagged Cx43t258 into the bleached region (Cx43K258stop-msfGFP in HeLa cells shown in this example; *scale bar*, 5 μm). A line scan (from the area of the GJ plaque indicated by the *yellow brackets*) shows the intensity profile of the bleach region to illustrate recovery. *B*, normalized FRAP curves indicate a difference between full-length Cx43 and Cx43 truncated at amino acid 258. *Orange trace*, Cx43t258-msfGFP in HeLa cells ($n = 3$). *Top gray trace*, Cx43t258-msfGFP in N2A cells ($n = 6$); *bottom red* and *gray traces*, full-length Cx43-msfGFP in HeLa and N2A cells ($n = 11$ and 6, respectively). *C*, percent recovery at 30 s postbleach is significantly higher for truncated Cx43 than full-length Cx43. *D*, border blur at 30 s is significantly higher for truncated Cx43. *E*, CT-localized non-monomerized sfGFP reduces percent recovery at 30 s and border blur at 30 s, whereas the effect of non-monomerized fluorescent protein is occluded when the fluorescent protein is tagged to the NT of truncated Cx43. Data for full-length Cx43-msfGFP are sourced from Fig. 3. *Error bars*, S.E. Groups were compared by ANOVA followed by Tukey's multiple comparison test. **, $p < 0.01$.
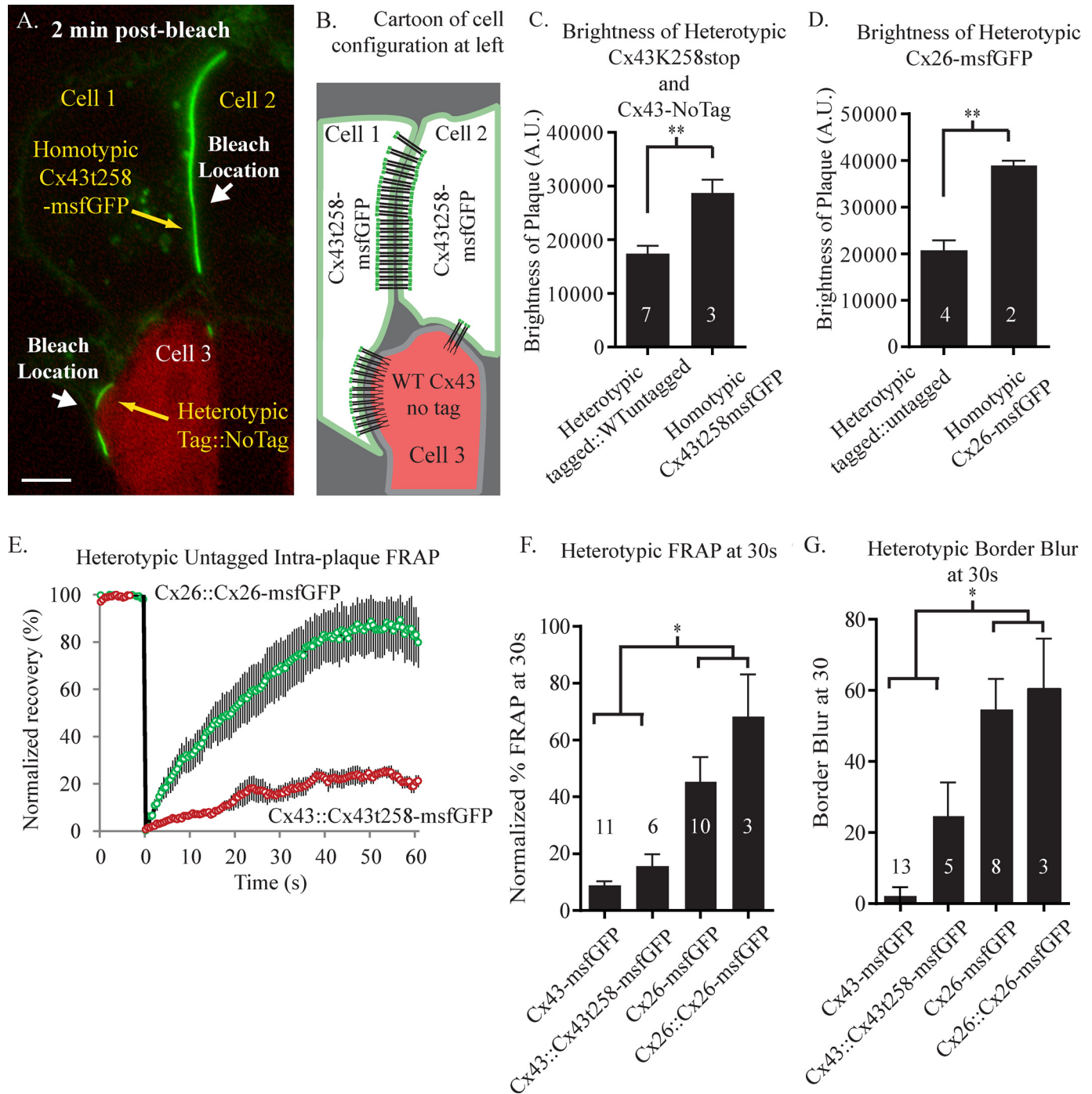
FIGURE 7. **Presence of a monomerized fluorescent protein tag does not qualitatively alter GJ plaque arrangement stability.** *A*, two separate HeLa cell cultures were transfected and then replated together. The image shows an example of pairs of cells in which cell 1 and cell 2 expressed Cx43t258-msfGFP. Cell 3 expressed mCherry, marking it as a cell from the culture that was transfected with full-length rat Cx43 without a fluorescent protein tag. This *panel* shows a single plane of a three-dimensional *Z*-stack performed 2 min after 2 μm of *both* the top and bottom plaques were bleached. The top plaque made up of homotypic Cx43t258-msfGFP has recovered fluorescence signal in the bleached region, but the untagged full-length Cx43 expressed by cell 3 has stabilized the heterotypic, lower plaque, thereby preventing recovery into the bleached region. *Scale bar*, 5 μm. *B*, schematic to clarify the position of cells and forms of Cx43 making up the plaque (not to scale). *C*, heterotypic tagged::untagged plaques are significantly dimmer than tagged::tagged plaques. *D*, heterotypic tagged::untagged (Cx26-msfGFP::Cx26) plaques are significantly dimmer than homotypic Cx26-msfGFP::Cx26-msfGFP plaques. *E*, FRAP recovery curves for heterotypic Cx43t258-msfGFP::untagged-Cx43 (*red circle markers*) and heterotypic Cx26-msfGFP::Cx26 (*green circle markers*). $n = 6$ and 3 for Cx43 and Cx26, respectively. *F* and *G*, untagged Cx43 stabilizes the arrangement of channels within the GJ, and untagged Cx26 is fluidly arranged within heterotypically tagged GJs. *, $p < 0.05$; **, $p < 0.01$. All groups in *C* and *D* were compared by Student's unpaired *t* test. Groups in *F* and *G* were compared by one-way ANOVA followed by Tukey's multiple comparison test. Data for homomeric tagged channels in *F* and *G* are sourced from Fig. 3. *A.U.*, arbitrary units.

figures for brevity. We found that sfGFP-Cx43 truncated at amino acid 244 also formed fluidly arranged plaques with an average recovery of 23 ± 3% and percent "bleach border blur" of

53 ± 3% at 30 s in seven experiments in HeLa cells. These results indicated that the CT of Cx43 stabilizes the arrangement of channels within GJs (Fig. 6). Similar results were obtained in

other connexin-deficient cell lines including N2A cells as shown in Fig. 6. Non-monomerized sfGFP tagged to the CT of Cx43K258stop had a stabilizing effect similar to that observed for Cx26 and Cx30, and this effect was lost when the non-monomerized sfGFP was transferred to the NT of Cx43K258stop (Fig. 6E), further supporting separate mechanisms of stabilization for endogenous Cx43 and "artificial stabilization" by non-monomerized fluorescent protein tags; results are summarized in Table 2.

Cx43 Stabilization of Gap Junction Channel Arrangement Does Not Depend on Fluorescent Protein Tag—We found that tagged or untagged Cx43K258stop formed plaques and paired with full-length Cx43 regardless of whether the full-length or truncated Cx43 was tagged (Fig. 7). This allowed us to test whether untagged Cx43 stabilized the normally fluidly arranged Cx43K258stop-msfGFP, and we found that such heterotypic Cx43::Cx43K258stop-msfGFP GJs were made up of stable plaques (Fig. 7 and summarized in Table 3). Untagged Cx43S257stop::Cx43K258stop-msfGFP formed fluidly arranged plaques (not shown). Likewise, when Cx43K258stop-msfGFP was co-expressed with full-length tagged (EBFP2-Cx43; not shown) or untagged Cx43, the resulting plaques were stably arranged (Fig.

7E). These results further indicate that msfGFP is not the mechanism behind Cx43 plaque arrangement stability. Co-expression of Cx43K258stop-msfGFP within the same cells as Cx43S257stop produced heteromeric plaques that were fluidly arranged, indicating that the msfGFP tag did not act as a lubricating agent for the channels within the plaque (Fig. 8). We found that heteromeric plaques made up of co-expressed Cx43-msfGFP with Cx43 (full-length, untagged) or with Cx43S257stop formed stably arranged plaques (Fig. 8).

The Fluorescent Protein Tags Do Not Lubricate Cx26 Channel Arrangement—We found that Cx26-msfGFP::Cx26(no tag) heterotypic GJs form fluidly arranged GJ plaques (Fig. 7, E–G). Cx26-msfGFP/Cx26 heteromeric GJs have similar arrangement dynamics as GJs purely composed of Cx26-msfGFP (Fig. 8, A and B). This indicates that space occupied by the fluorescent protein tag is not the cause of the fluid arrangement of Cx26 GJs.

Fluorescent Protein Tag Strongly Affects Heterotypic Plaque Arrangement—Because we observed strong effects of fluorescent protein tag type and location on the stability of GJ arrangement within the plaque, we went on to test whether fluorescent protein tags also affect the arrangement of the plaque when multiple connexin types were present within the same plaque. For these tests, we used enhanced blue fluorescent protein-tagged connexins co-transfected with msfGFP- or sfGFP-tagged connexins. Previous reports using non-monomerized, CT fluorescent protein tags indicated that Cx26 and Cx43 are maintained within spatially separated pools of GJs at the same plaque structure (6). When EBFP2-Cx43 was co-transfected with Cx26-sfGFP or with Cx30-sfGFP, the resulting plaques formed segregated structures, as shown in Fig. 9 (A and B). These observations are in agreement with previous reports and the current concept of GJ arrangement at the plaque as reviewed by Koval *et al.* (13). However, when we co-transfected EBFP2-Cx43 with Cx26-msfGFP (or with Cx26-mVenus; not shown) or with Cx30-msfGFP, we observed mixed plaques (Fig. 9, C and D). In parallel with decreasing plaque arrangement stability, translocation of sfGFP from the CT to the NT of Cx26 and Cx30 converted the plaque to the intermingled morphology when co-expressed with Cx43 (Fig. 9, E and F). Even in combinations in which connexins formed intermingled

TABLE 3
Additional FRAP results- un-tagged connexins to test for more endogenous-like behavior

Connexin and Tag	Expected topology at GJ plaques	Stable or Fluid channel arrangement	Figure	Cell types tested
Heterotypic Cx43 + Cx43K258stop-msfGFP		Stable	Fig.7	HeLa, N2A[a]
Heterotypic Cx26 + Cx26-msfGFP		Fluid	Fig.7	HeLa, N2A[a]
Heteromeric Cx43 + Cx43-msfGFP		Stable	Fig.8A,B	HeLa
Heteromeric Cx26 + Cx26-msfGFP		Fluid	Fig.8A,B	HeLa
Heteromeric Cx43S257stop + Cx43K258stop-msfGFP		Fluid	Fig.8A,B	HeLa
Heteromeric Cx43S257stop + Cx43-msfGFP		Stable	Fig.8C	HeLa

[a] Results for these heterotypic FRAP experiments were validated in 1–2 trials each, in N2A cells using CellTracker Orange CMTMR loaded into the cells that received transfection of untagged connexin expression plasmids. The cells labeled with CellTracker dye were then washed, and the cells were replated with cells transfected with msfGFP-tagged connexin. This avoids any possible interaction of the untagged connexin with the fluorescent protein because there was none in the N2a cells expressing untagged connexin.
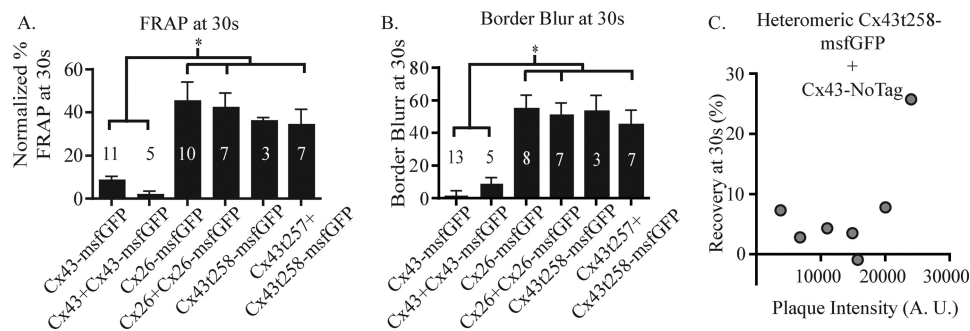
FIGURE 8. **Mobility of untagged connexins in heteromeric complexes is similar to that of tagged connexins.** *A*, percent FRAP at 30 s for heteromeric tagged/untagged GJs is similar to GJs formed in cells only transfected with tagged connexins as in Figs. 3 and 6. Data for homomeric msfGFP-tagged connexins are sourced from Fig. 3. *B*, bleach border analysis indicates an amount of GJ channel rearrangement for GJ plaques only partially tagged (also known as heteromerically tagged) is similar to that for fully tagged plaques (also known as homomerically tagged, as in Figs. 1–5). *C*, percent recovery at 30 s is not correlated to plaque intensity for heteromeric Cx43t258-msfGFP/Cx43 plaques (even when a potential outlier is removed), indicating that only a small percentage of channels required an intact CT in heteromeric (truncated/full-length) plaques to form a stable channel arrangement. Note that data points shown in *C* are from an experimental group different from that represented in *A* and *B*. *A.U.*, arbitrary units. Groups were compared by ANOVA followed by Tukey's multiple comparisons test. *, $p < 0.05$.
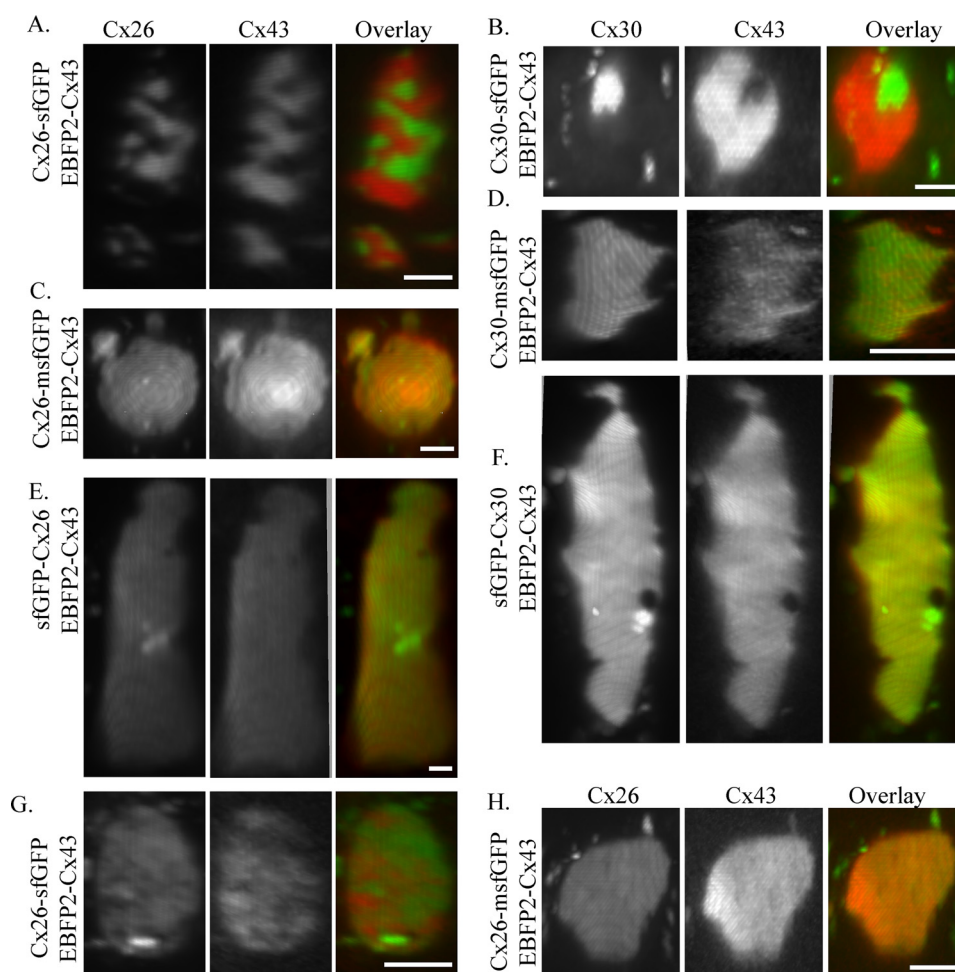
FIGURE 9. **Fluorescent protein tag dimerization is the cause of large scale segregation of GJs within mixed type plaques.** *A*, when Cx26-sfGFP (non-mono-merized FP tag) is co-expressed with EBFP2-Cx43, the two types of GJs are segregated to nearly mutually exclusive domains. *B*, when Cx30-sfGFP is expressed with EBFP2-Cx43, it also forms Cx type-specific, large clusters. *C*, when Cx26 tagged with monomerized sfGFP is co-expressed with EBFP2-Cx43, the two types of GJ intermingle within the plaque (but not in the Golgi apparatuses or ER complexes as shown in supplemental movies 8 and 11. *D*, replacing sfGFP with msfGFP as the tag on Cx30 has a similar intermingling effect on the arrangement of plaques made up of Cx30 and EBFP2-Cx43. *E* and *F*, relocating the original sfGFP from the CT to the NT of Cx30 and Cx26 has a similar effect on plaque intermingling with EBFP2-Cx43 as it does on mobility, probably due to relocation toward the pore of the GJ channel and prevention of the sfGFP from dimerizing with an sfGFP tag on a neighboring channel. *G*, non-monomerized Cx26-sfGFP forms separate regions within Cx43/Cx26 mixed plaques in N2A cells. *H*, when Cx26-msfGFP and EBFP2-Cx43 are co-transfected into N2A cells, the resulting plaques are well mixed with respect to connexin type. Images in *A–F* are of HeLa cells, and images in *G* and *H* are of N2A cells. *Scale bars* (*A*, *B*, *G*, and *H*), 2 μm; *scale bars* (*C–F*), 5 μm.

plaques, we observed well separated intracellular punctate structures, probably representing distinct pools of nascent Cx26/Cx30 in separate vesicles from Cx43 en route to the plasma membrane, indicating that Cx43 subunits do not form heteromeric GJs even in intermingled plaques, in agreement with previous reports (9, 36, 37) and illustrated in supplemental Movie 8. Immunostaining of untagged Cx43 co-expressed with Cx26-msfGFP and Cx26-sfGFP yielded similar results as with tagged Cx43 (Fig. 10, *A* and *B*). When cells expressing untagged Cx43 and Cx26 were immunostained, intermingled plaques were observed (Fig. 10, *A–D*) with some clustering of untagged connexins observed in some other cases (see Table 4). When EBFP2-Cx26 or EBFP2-Cx30 were co-expressed with Cx43-sf-GFP, segregated plaques formed (Fig. 10*E*), but when EBFP2-tagged β class connexins Cx30 and Cx26 were co-expressed with Cx43-msfGFP, intermingled plaques formed (Fig. 10*F*), but very small clusters of Cx43-msfGFP were observed. Inter-estingly, in this case, the large Cx43-sfGFP clusters localized to the center of the plaques in contrast to when EBFP2-Cx43

is co-expressed with Cx30-sfGFP, further indicating that dimerization of the sfGFP is the mechanism behind formation of large clusters; results are summarized in Table 4. When EBFP2-Cx26 and Cx30-sfGFP were co-transfected, they formed intermingled fluorescence both at the plaque structure *and* in intracellular puncta, probably due to heteromeric chan-nel formation (not shown), as described previously (6); how-ever, demonstration of heteromeric or homomeric connexin formation has not been accomplished through optical micros-copy but has been demonstrated previously through biochem-ical and electrophysiological methods (36, 37). Gong *et al.* (38) raised the possibility that untagged Cx43 and EGFP-Cx32 might form intermingled plaques in an earlier study. In sum-mary, consistent arrangement of GJs into large well defined clusters, according to class, at the same plaque structure is caused by attachment of a non-monomerized fluorescent pro-tein tag on the CT of one of the two connexins, at least in the case of Cx43, Cx30, and Cx26.
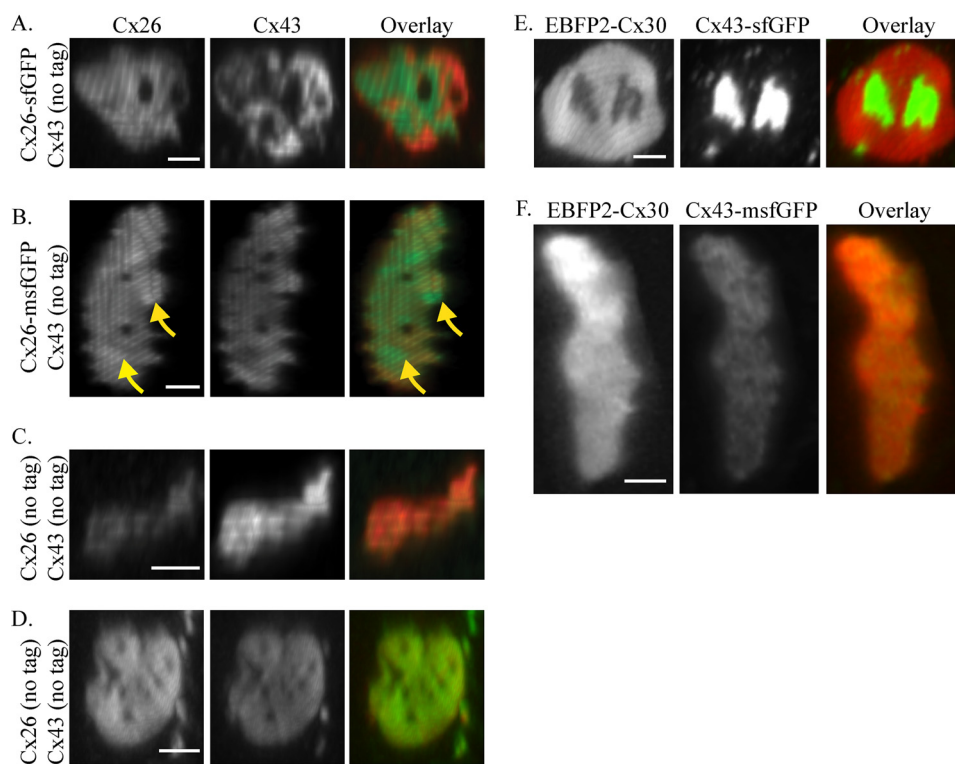
FIGURE 10. **Fluorescent protein clustering and intermingling without fluorescent protein tags on one or both connexins.** *A*, when immunostained Cx43 and Cx26-sfGFP are localized to the same plaque, they are segregated to mostly non-overlapping domains. *B*, when untagged Cx43 is co-expressed with Cx26-msfGFP, however, more intermixing takes place, although some regions with more or less Cx26 can be observed (*yellow arrows*). *C*, intermixing of untagged Cx26 and Cx43. *D*, intermixing of untagged Cx26 and Cx43 is also observed in N2A cells overexpressing untagged connexins. *Red*, Cx43 (Alexa594-labeled secondary). *Green*, Cx26-GFP (*A* and *B*) and Alexa488 labeling of Cx26 (*C* and *D*). *E*, when NT-tagged Cx30 (EBFP2-Cx30) is co-expressed with Cx43-sfGFP, the two GJ types are localized to separate regions within the plaque. Interestingly, in this case, the Cx43-sfGFP is localized to the center of the plaque, whereas Cx43 localizes throughout the plaque when EBFP2-Cx43 is co-expressed with Cx26-sfGFP or Cx30-sfGFP. *F*, when EBFP2-Cx30 is co-expressed with Cx43-msfGFP, the channels intermingle, but there may be some Cx43-msfGFP grouping that occurs, leading to small clustered structures near the resolution limit of standard light microscopy. Images in *A–C* and *E–F* are of HeLa cells, and images in *D* are of N2A cells. *Scale bar*, 2 μm.

Discussion

We show that multiple factors affect the stability of GJ plaques. Our demonstration of dynamic Cx26, Cx30, and Cx43K258stop plaque arrangements establishes that plaque arrangement stability is not required for the formation of large plaques. This finding is important for models of GJ organization and has implications for understanding how GJs form and how tissues regulate cell-cell interactions.

We never observed blurring of the bleach border produced within full-length Cx43 plaques, even when they were examined 1 h after the bleaching event. Because the average total time that each Cx43 protein is part of the GJ plaque structure has been estimated to be less than 3 h (39–42), our results indicate that the arrangement of GJ channels within the plaque structure of Cx43 GJs does not change during the "in-plaque lifetime" of the Cx43 channels. Thus, Cx43 "arrangement stability within the plaque" is not a relative term. We find that Cx43 forms statically arranged GJ plaques, whereas Cx30 and Cx26 form highly fluidly arranged ones. Our findings that Cx43 is always statically arranged and Cx26 GJs are extremely fluid contrast with the observation of two distinct populations (static and dynamically arranged) for both Cx43 and Cx26 by Simek *et al.* (4). These differences may be due to experimental FRAP conditions or analysis methods, such as our three-dimensional reconstructions of FRAP regions that correct for whole plaque

movement that otherwise may be interpreted as dynamic plaque arrangement.

A curious aspect of statically arranged Cx43 GJ plaques is that substantial changes to the overall shape of the plaque can occur while a sharp photobleach-generated border is maintained. This fits with the concept that Cx43 GJ arrangement is maintained by abundant weak/transient interactions between neighboring channels while the overall plaque structure is malleable. Therefore, we hypothesize that this unusual plaque behavior is achieved through non-covalent lateral interactions between neighboring Cx43 channels or through binding to an extensive cytoplasmic scaffold. This idea is supported by our demonstration that plaque arrangement stability is completely eliminated when most of the cytoplasmic CT of Cx43 is removed. Simek *et al.* (4) noted an increase in the percentage of mobile GJs for a different Cx43 truncation (Cx43 truncated at amino acid 244). Using monomeric fluorescent proteins, we observed a qualitative switch from stable arrangement to fluid arrangement with truncation of Cx43 at either amino acid 258 or 245. This indicates that plaque stability is probably produced by a binding interaction of the Cx43 CT to C termini of adjacent Cx43 channels or to a cytoplasmic scaffold. Truncation of the CT of Cx43 does reduce the molecular mass of the connexin from 43.03 to 29.44 kDa. We show that the Cx43t258-msfGFP::Cx43-untagged plaques (estimated

TABLE 4

Summary of observations on heterotypic intermingling of co-expressed connexins

Connexins co-expressed	Expected channel topology drawing	Non-mixed plaques / plaques examined	Avg. diameter of GJs examined (μm)
EBFP2-Cx43 + Cx26-sfGFP		9/9 HeLa 6/6 N2A	5 9
EBFP2-Cx43 + Cx26-msfGFP		0/3 HeLa 0/6 N2A	7 8
EBFP2-Cx43 + Cx30-sfGFP		5/5	6
EBFP2-Cx43 + Cx30-msfGFP		0/7	5
EBFP2-Cx43 + sfGFP-Cx26		0/8	6
EBFP2-Cx43 + sfGFP-Cx30		0/4	10
EBFP2-Cx26 + Cx43-sfGFP		6/7	9
EBFP2-Cx30 + Cx43-sfGFP		13/17[a]	7
EBFP2-Cx30 + Cx43-msfGFP		0/9	8
untaggedCx43 + Cx26-sfGFP		15/18	8
untaggedCx43 + Cx26-msfGFP		0/15[b]	10
untaggedCx43 + untaggedCx26		0/5 HeLa 1/8 N2A	4 6

[a] Cx43-sfGFP co-expressed with EBFP-Cx30 led to separated clusters of Cx43-sfGFP that were smaller and more numerous than those observed when Cx30-sfGFP was co-expressed with EBFP2-Cx43. In the four GJs where Cx43-sfGFP appeared to intermingle with EBFP2-Cx30 there appeared to be very small clusters of Cx43-sfGFP near the resolution of the microscope (~250 nm).

[b] Some GJ plaques (4 of 15) made up of untagged Cx43 and Cx26-msfGFP had small areas at the edge of the plaque with only green (Cx26-msfGFP) signal, but in all of these four cases, the rest of the adjacent plaque area next to these small areas was always well mixed for the two colors.

molecular mass per channel = 602 kDa) are stably arranged, whereas homotypic Cx43t258-msfGFP::Cx43t258-msfGFP channels (estimated molecular mass per channel = 687 kDa) form fluid plaques, indicating that nonspecific increased size is not the mechanism behind Cx43 stability (Figs. 7 and 8), as described previously for mobility characteristics of other membrane proteins (43, 44).

We found that non-monomerized GFP can stabilize channel arrangement in normally fluidly arranged GJs. Taken together, the results of the experiments described here indicate that stability of Cx43 imparted by the CT of the connexin is a separate endogenous stabilizing factor for GJ channel arrangement, whereas, in contrast, stability imparted by CT-localized non-monomerized GFP is an experimental artifact. Fusion of the fluorescent fusion protein tag to the N terminus of connexins prevents artificial stabilization. This probably occurs due to the non-monomerized sfGFP no longer interacting with and weakly binding to sfGFP molecules attached to neighboring GJ channels. The NT of connexins are thought to be situated within the pore of GJs (35), whereas the CTs are localized to the cytoplasm at a more medial position on the channel (illustrated in Fig. 5, *A* and *B*). Therefore, we propose that the sfGFP tagged onto the Cx26 NT (or Cx43K258stop NT) is repositioned away from sfGFP on neighboring GJ channels, thereby sterically blocked from binding, preventing GJ channel lateral clumping and plaque stabilization. The finding that placing the tag on the NT of connexins prevents stabilizing artifacts of GFP may be useful to rule out dimerization effects of other tags, such as

photoconvertible proteins that have been used in studies on GJ dynamics (7) and structure (8). It may also be important to test newly developed fluorescent proteins as tags on connexins by appending them to both the NT and separately to the CT of fluidly arranged connexins, such as Cx26, and then comparing mobility with FRAP.

It should be noted that all normally functional connexins so far tested with NT fluorescent protein tags form GJ plaque structures but do not allow dye or electrical coupling (45). This lack of channel function is thought to be due to the NT normally contributing to the GJ channel pore and the fluorescent protein tag at that location somehow disrupting functional channel formation (14, 35, 46). Therefore, NT-tagged connexins cannot substitute for monomerized fluorescent protein CT connexin tags when both "normal plaque structural dynamics" and some channel function are desired. Conversely, CT tags on connexins lead to altered gating, plaque size, and interactions with cytoplasmic binding partners, such as ZO-1 (14, 47). Loss of Cx43 interaction with ZO-1 has been shown to increase GJ plaque size. This appears to be a partial cause of the highly enlarged GJs seen in cultured cells overexpressing connexins but is not likely to be the sole cause because we observed enlarged plaques in cells expressing NT-tagged and untagged Cx43. Cx43 tagged with EGFP on the NT has been shown to interact with ZO-1 (48) and both full-length sfGFP-Cx43 and sfGFP-Cx43t258 overexpression led to abnormally large plaques in more than one cell type (Fig. 6 and Table 4). In summary, we conclude that no fluorescent protein-tagged connexin is optimal for every experimental design, that fluorescent protein tag type and location should be carefully considered for each particular experimental paradigm, and that the monomeric characteristics of a fluorescent protein can significantly impact the localization and dynamics of oligomeric integral membrane proteins.

Standard resolution confocal light microscopy cannot resolve single GJ channels. Therefore, we cannot differentiate heteromeric GJ channels within plaques from intermingled homotypic channels. Biochemical analysis techniques are better suited for these particular tests. Such work by others indicated that Cx43 and Cx30/Cx26 connexins do not form heteromeric channels (11, 49), and consistent results were obtained for other similar connexin combinations (38). The high overexpression of connexins can saturate and overcome cellular control of connexin oligomerization (50). However, there was apparently enough control of Cx43 oligomerization in our experimental conditions to allow separate oligomerization when sfGFP dimerization produces segregated plaques. Additionally, saturation of oligomerization control does not account for differences produced by single amino acid changes to the fluorescent protein tag, as shown in Fig. 9.

The finding that the position of the non-monomerized fluorescent protein tag affects mobility could indicate that mobility might be influenced by the length or flexibility of the linker. However, when monomeric fluorescent protein tags were used, similar mobility characteristics were observed for both stably arranged (Cx43) and fluid (Cx26) connexins regardless of the tag location, indicating that with improved fluorescent protein tags, tag location and consequently the size and sequence of the

linker (within a reasonable range) do not substantially affect mobility.

A related caveat of the present study is that GFP and other fluorescent proteins are relatively large (5-nm) additions. The molecular weight of GFP is similar to those of Cx26 and Cx30 and nearly half the weight of Cx43. In the highly crowded environment of the GJ plaque, GFP might be expected to affect movement of GJ channels within the membrane. Indeed, the trafficking and assembly of connexins into GJs can be altered by the addition of fluorescent protein tags (5, 47). We found that when tagged and untagged connexins were mixed, the apparent dynamics of the resulting channel arrangement was not significantly affected. Heteromeric tagged::untagged Cx26 and Cx43 truncation constructs exhibited significantly increased mobility compared with full-length Cx43. These results also established that the fluidity observed for Cx26, Cx30, and Cx43K258stop is unrelated to the fluorescent protein tag. The experiments with tagged::untagged connexins indicate that FRAP with msfGFP-tagged connexins can reveal the characteristics of untagged connexins (at least in the case of transgenic overexpression; see below).

The abnormally large plaques formed by overexpression of connexins in cultured cells contrast with the smaller plaques that form *in vivo* (~0.01–2.0 μm) (51). However, the dynamic characteristics that we uncovered here are expected to be relevant for *in vivo* GJ structure because the arrangement stability of Cx43 channels was dependent on amino acids within the CT of Cx43 and was maintained by Cx43 without a fluorescent protein tag (Figs. 7 and 8). Stability is an intrinsic property of Cx43 channels and not present in GJs composed of Cx26 and Cx30. In addition, the mobility characteristics that we report were features of GJs ranging from 4 μm to more than 20 μm in diameter and were maintained at both the center and perimeter of the plaques (Fig. 3*D* and three-dimensional reconstructions shown in supplemental Movies 2–6). Despite these caveats, our results provide new insights into GJ arrangement stability and plaque structure and how these properties are modified by connexin type, fluorescent protein tag type, and tag location. Our findings also indicate that the CT is required for the formation of stable Cx43 GJ plaques.

We also conclude that the sharp segregation of Cx43 and Cx26 within the same plaque reported previously was a result of aggregation of CT, non-monomerized tags. Non-mixed GJ plaques readily form when non-monomerized tags are used (Fig. 9, *A* and *B*) (6). To potentially explain the underlying mechanism, we considered all of the different combinations of tag location and tag type examined in this study (Table 4), and we formulated the following hypothesis. We propose that strong lateral interactions are needed to form non-intermingled GJs as with sfGFP dimerization in EBFP2-Cx43 + Cx26-sfGFP GJs (Fig. 9, *A* and *B*), and an imbalance is required between the strength of lateral interactions between the two Cx tag types that present in the GJ. We hypothesize that clustering according to Cx tag type occurs as new GJ channels form at the edge of the plaque. If the drive to cluster is strong (as with Cx26-sfGFP), this strong clustering "squeezes out" the weaker lateral interactions of the Cx43 channels, at the very local level of the plaque periphery. Once

the channels are fully clustered into the plaque structure, they would be locked into their arrangement by the stably arranged Cx43, according to this scenario. If this hypothesized mechanism behind intermingled and non-intermingled plaques is correct, then segregated plaques could form *in vivo* if Cx43 expression preceded that of Cx26 or Cx30. Therefore, the present study does not rule out the formation of unmixed GJ plaques *in vivo*, but we do show that non-monomerized fluorescent proteins strongly interfere with tests aimed at investigating this intriguing model.

NT-tagged connexins might be most appropriate for future studies aimed at examination of connexin plaque arrangement stability and/or arrangement of binding partners at the GJ plaque. NT-tagged connexins have proven useful in this regard in previous studies (48, 52–55). If channel activity is required, the msfGFP CT tags are probably the current best choice.

The connexins examined here (Cx43, Cx30, and Cx26) are co-expressed in astrocytes in the mammalian brain. Each connexin type has different channel properties; binds unique sets of cellular proteins; and has different regulation of expression, trafficking, and activity. Therefore, our results will be important as we achieve finer resolution mapping of astrocyte connectivity within the brain. This study demonstrates that the mobility and arrangement of Cx26 and Cx30 are affected by fluorescent protein tag type, and this finding should be taken into account for studies using fluorescent protein fusion constructs as localization markers in highly crowded and ordered cellular compartments. Several recent reports have indicated that the arrangement of certain phosphorylated Cx43 GJs is regulated and spatially segregated within the plaque (18, 19). We hypothesize that the stability that we observed for Cx43 plaques is important for localization of specific posttranslational modification of GJs to appropriate subregions of Cx43 GJ plaques. This raises the exciting possibility that cells express multiple connexin types to allow differential GJ arrangement stability. Cx43 and Cx30 were recently shown to have differential tissue distribution in the mouse visual cortex, and this distribution is correlated with functional organization of cortical brain tissue, at least in layer IV of this region of the cerebral cortex (56). Deletion of astrocyte Cx30 alone and deletion of both Cx43 and Cx30 were shown to have opposite effects on synaptic transmission and plasticity (57, 58). These differences in neuronal activity were ascribed to channel-independent effects of the Cx30 CT. Additionally, Cx43 and Cx30 are highly localized to the astrocyte process that wraps specifically around brain vasculature (known as the astrocyte endfoot domain). Other integral membrane proteins, such as AQP4 and Kir4.1, are highly localized to the same area where Cx43 and Cx30 plaques cluster in the endfoot. Localization of AQP4 and Kir4.1 to the astrocyte endfoot has been shown to be important in the pathological manifestation of mouse models of neural disease and human brain samples (59–65). We speculate that different properties imparted to the endfoot and perisynaptic domains of astrocytes by stable or fluid GJ plaques affect astrocyte morphology and localization of other proteins that are required for brain homeostasis, including AQP4 and Kir4.1. Alterations to astrocyte connexin expression and localization have been

reported for most neurological diseases (60, 64, 66–70). Results that we present in this study may be important for improving our understanding of how alteration to astrocyte connexin expression, localization, and function fit into the etiology of complex neurological disorders.

References

1. Shimomura, O., Johnson, F. H., and Saiga, Y. (1962) Extraction, purification and properties of aequorin, a bioluminescent protein from the luminous hydromedusan, Aequorea. *J. Cell Comp. Physiol.* **59,** 223–239
2. Chalfie, M., Tu, Y., Euskirchen, G., Ward, W. W., and Prasher, D. C. (1994) Green fluorescent protein as a marker for gene expression. *Science* **263,** 802–805
3. Heim, R., Cubitt, A. B., and Tsien, R. Y. (1995) Improved green fluorescence. *Nature* **373,** 663–664
4. Simek, J., Churko, J., Shao, Q., and Laird, D. W. (2009) Cx43 has distinct mobility within plasma-membrane domains, indicative of progressive formation of gap-junction plaques. *J. Cell Sci.* **122,** 554–562
5. Thomas, T., Jordan, K., Simek, J., Shao, Q., Jedeszko, C., Walton, P., and Laird, D. W. (2005) Mechanisms of Cx43 and Cx26 transport to the plasma membrane and gap junction regeneration. *J. Cell Sci.* **118,** 4451–4462
6. Falk, M. M. (2000) Connexin-specific distribution within gap junctions revealed in living cells. *J. Cell Sci.* **113,** 4109–4120
7. Falk, M. M., Baker, S. M., Gumpert, A. M., Segretain, D., and Buckheit, R. W., 3rd (2009) Gap junction turnover is achieved by the internalization of small endocytic double-membrane vesicles. *Mol. Biol. Cell* **20,** 3342–3352
8. Baker, S. M., Buckheit, R. W., 3rd, and Falk, M. M. (2010) Green-to-red photoconvertible fluorescent proteins: tracking cell and protein dynamics on standard wide-field mercury arc-based microscopes. *BMC Cell Biol.* **11,** 15
9. Musil, L. S., and Goodenough, D. A. (1993) Multisubunit assembly of an integral plasma membrane channel protein, gap junction connexin43, occurs after exit from the ER. *Cell* **74,** 1065–1077
10. Falk, M. M., Kumar, N. M., and Gilula, N. B. (1994) Membrane insertion of gap junction connexins: polytopic channel forming membrane proteins. *J. Cell Biol.* **127,** 343–355
11. Das Sarma, J., Wang, F., and Koval, M. (2002) Targeted gap junction protein constructs reveal connexin-specific differences in oligomerization. *J. Biol. Chem.* **277,** 20911–20918
12. Fort, A. G., Murray, J. W., Dandachi, N., Davidson, M. W., Dermietzel, R., Wolkoff, A. W., and Spray, D. C. (2011) *In vitro* motility of liver connexin vesicles along microtubules utilizes kinesin motors. *J. Biol. Chem.* **286,** 22875–22885
13. Koval, M., Molina, S. A., and Burt, J. M. (2014) Mix and match: investigating heteromeric and heterotypic gap junction channels in model systems and native tissues. *FEBS Lett.* **588,** 1193–1204
14. Bukauskas, F. F., Jordan, K., Bukauskiene, A., Bennett, M. V., Lampe, P. D., Laird, D. W., and Verselis, V. K. (2000) Clustering of connexin 43-enhanced green fluorescent protein gap junction channels and functional coupling in living cells. *Proc. Natl. Acad. Sci. U.S.A.* **97,** 2556–2561
15. Holm, I., Mikhailov, A., Jillson, T., and Rose, B. (1999) Dynamics of gap junctions observed in living cells with connexin43-GFP chimeric protein. *Eur. J. Cell Biol.* **78,** 856–866
16. Jordan, K., Solan, J. L., Dominguez, M., Sia, M., Hand, A., Lampe, P. D., and Laird, D. W. (1999) Trafficking, assembly, and function of a connexin43-green fluorescent protein chimera in live mammalian cells. *Mol. Biol. Cell* **10,** 2033–2050
17. Windoffer, R., Beile, B., Leibold, A., Thomas, S., Wilhelm, U., and Leube, R. E. (2000) Visualization of gap junction mobility in living cells. *Cell Tissue Res.* **299,** 347–362
18. Dunn, C. A., and Lampe, P. D. (2014) Injury-triggered Akt phosphorylation of Cx43: a ZO-1-driven molecular switch that regulates gap junction size. *J. Cell Sci.* **127,** 455–464
19. Cone, A. C., Cavin, G., Ambrosi, C., Hakozaki, H., Wu-Zhang, A. X., Kunkel, M. T., Newton, A. C., and Sosinsky, G. E. (2014) Protein kinase Cδ-mediated phosphorylation of Connexin43 gap junction channels causes movement within gap junctions followed by vesicle internalization and protein degradation. *J. Biol. Chem.* **289,** 8781–8798
20. Ai, H. W., Shaner, N. C., Cheng, Z., Tsien, R. Y., and Campbell, R. E. (2007) Exploration of new chromophore structures leads to the identification of improved blue fluorescent proteins. *Biochemistry* **46,** 5904–5910
21. Nagai, T., Ibata, K., Park, E. S., Kubota, M., Mikoshiba, K., and Miyawaki, A. (2002) A variant of yellow fluorescent protein with fast and efficient maturation for cell-biological applications. *Nat. Biotechnol.* **20,** 87–90
22. Nakagawa, C., Nishimura, S., Senda-Murata, K., and Sugimoto, K. (2012) A rapid and simple method of evaluating the dimeric tendency of fluorescent proteins in living cells using a truncated protein of importin α as fusion tag. *Biosci. Biotechnol. Biochem.* **76,** 388–390
23. Zacharias, D. A., Violin, J. D., Newton, A. C., and Tsien, R. Y. (2002) Partitioning of lipid-modified monomeric GFPs into membrane microdomains of live cells. *Science* **296,** 913–916
24. Snapp, E. L., Hegde, R. S., Francolini, M., Lombardo, F., Colombo, S., Pedrazzini, E., Borgese, N., and Lippincott-Schwartz, J. (2003) Formation of stacked ER cisternae by low affinity protein interactions. *J. Cell Biol.* **163,** 257–269
25. Pédelacq, J. D., Cabantous, S., Tran, T., Terwilliger, T. C., and Waldo, G. S. (2006) Engineering and characterization of a superfolder green fluorescent protein. *Nat. Biotechnol.* **24,** 79–88
26. Snapp, E. L., Altan, N., and Lippincott-Schwartz, J. (2003) Measuring protein mobility by photobleaching GFP chimeras in living cells. *Curr. Protoc. Cell Biol.* 10.1002/0471143030.cb2101s19
27. Snapp, E. L., and Lajoie, P. (2011) Photobleaching regions of living cells to monitor membrane traffic. *Cold Spring Harb. Protoc.* **2011,** 1366–1367
28. Schneider, C. A., Rasband, W. S., and Eliceiri, K. W. (2012) NIH Image to ImageJ: 25 years of image analysis. *Nat. Methods* **9,** 671–675
29. Schindelin, J., Arganda-Carreras, I., Frise, E., Kaynig, V., Longair, M., Pietzsch, T., Preibisch, S., Rueden, C., Saalfeld, S., Schmid, B., Tinevez, J. Y., White, D. J., Hartenstein, V., Eliceiri, K., Tomancak, P., and Cardona, A. (2012) Fiji: an open-source platform for biological-image analysis. *Nat. Methods* **9,** 676–682
30. Sbalzarini, I. F., Mezzacasa, A., Helenius, A., and Koumoutsakos, P. (2005) Effects of organelle shape on fluorescence recovery after photobleaching. *Biophys. J.* **89,** 1482–1492
31. Eckert, R., Dunina-Barkovskaya, A., and Hülser, D. F. (1993) Biophysical characterization of gap-junction channels in HeLa cells. *Pflugers Arch.* **424,** 335–342
32. Costantini, L. M., and Snapp, E. L. (2013) Fluorescent proteins in cellular organelles: serious pitfalls and some solutions. *DNA Cell Biol.* **32,** 622–627
33. von Stetten, D., Noirclerc-Savoye, M., Goedhart, J., Gadella, T. W., Jr., and Royant, A. (2012) Structure of a fluorescent protein from *Aequorea victoria* bearing the obligate-monomer mutation A206K. *Acta Crystallogr. Sect. F Struct. Biol. Cryst. Commun.* **68,** 878–882
34. Maeda, S., Nakagawa, S., Suga, M., Yamashita, E., Oshima, A., Fujiyoshi, Y., and Tsukihara, T. (2009) Structure of the connexin 26 gap junction

channel at 3.5 Å resolution. *Nature* **458,** 597– 602

35. Oshima, A., Tani, K., Hiroaki, Y., Fujiyoshi, Y., and Sosinsky, G. E. (2007) Three-dimensional structure of a human connexin26 gap junction channel reveals a plug in the vestibule. *Proc. Natl. Acad. Sci. U.S.A.* **104,** 10034 –10039

36. Gemel, J., Valiunas, V., Brink, P. R., and Beyer, E. C. (2004) Connexin43 and connexin26 form gap junctions, but not heteromeric channels in co-expressing cells. *J. Cell Sci.* **117,** 2469 –2480

37. Beyer, E. C., Gemel, J., Martínez, A., Berthoud, V. M., Valiunas, V., Moreno, A. P., and Brink, P. R. (2001) Heteromeric mixing of connexins: compatibility of partners and functional consequences. *Cell Commun. Adhes.* **8,** 199 – 204

38. Gong, X. Q., Shao, Q., Langlois, S., Bai, D., and Laird, D. W. (2007) Differential potency of dominant negative connexin43 mutants in oculodentodigital dysplasia. *J. Biol. Chem.* **282,** 19190 –19202

39. Laird, D. W., Puranam, K. L., and Revel, J. P. (1991) Turnover and phosphorylation dynamics of connexin43 gap junction protein in cultured cardiac myocytes. *Biochem. J.* **273,** 67–72

40. Traub, O., Look, J., Paul, D., and Willecke, K. (1987) Cyclic adenosine monophosphate stimulates biosynthesis and phosphorylation of the 26 kDa gap junction protein in cultured mouse hepatocytes. *Eur. J. Cell Biol.* **43,** 48 –54

41. Beardslee, M. A., Laing, J. G., Beyer, E. C., and Saffitz, J. E. (1998) Rapid turnover of connexin43 in the adult rat heart. *Circ. Res.* **83,** 629 – 635

42. Fallon, R. F., and Goodenough, D. A. (1981) Five-hour half-life of mouse liver gap-junction protein. *J. Cell Biol.* **90,** 521–526

43. Marguet, D., Spiliotis, E. T., Pentcheva, T., Lebowitz, M., Schneck, J., and Edidin, M. (1999) Lateral diffusion of GFP-tagged H2Ld molecules and of GFP-TAP1 reports on the assembly and retention of these molecules in the endoplasmic reticulum. *Immunity* **11,** 231–240

44. Nikonov, A. V., Snapp, E., Lippincott-Schwartz, J., and Kreibich, G. (2002) Active translocon complexes labeled with GFP-Dad1 diffuse slowly as large polysome arrays in the endoplasmic reticulum. *J. Cell Biol.* **158,** 497–506

45. Laird, D. W., Jordan, K., Thomas, T., Qin, H., Fistouris, P., and Shao, Q. (2001) Comparative analysis and application of fluorescent protein-tagged connexins. *Microsc. Res. Tech.* **52,** 263–272

46. Kyle, J. W., Minogue, P. J., Thomas, B. C., Domowicz, D. A., Berthoud, V. M., Hanck, D. A., and Beyer, E. C. (2008) An intact connexin N-terminus is required for function but not gap junction formation. *J. Cell Sci.* **121,** 2744 –2750

47. Hunter, A. W., Jourdan, J., and Gourdie, R. G. (2003) Fusion of GFP to the carboxyl terminus of connexin43 increases gap junction size in HeLa cells. *Cell Commun. Adhes.* **10,** 211–214

48. Chen, J., Pan, L., Wei, Z., Zhao, Y., and Zhang, M. (2008) Domain-swapped dimerization of ZO-1 PDZ2 generates specific and regulatory connexin43-binding sites. *EMBO J.* **27,** 2113–2123

49. Smith, T. D., Mohankumar, A., Minogue, P. J., Beyer, E. C., Berthoud, V. M., and Koval, M. (2012) Cytoplasmic amino acids within the membrane interface region influence connexin oligomerization. *J. Membr. Biol.* **245,** 221–230

50. Das Sarma, J., Das, S., and Koval, M. (2005) Regulation of connexin43 oligomerization is saturable. *Cell Commun. Adhes.* **12,** 237–247

51. Rash, J. E., Duffy, H. S., Dudek, F. E., Bilhartz, B. L., Whalen, L. R., and Yasumura, T. (1997) Grid-mapped freeze-fracture analysis of gap junctions in gray and white matter of adult rat central nervous system, with evidence for a "panglial syncytium" that is not coupled to neurons. *J. Comp. Neurol.* **388,** 265–292

52. Bejarano, E., Girao, H., Yuste, A., Patel, B., Marques, C., Spray, D. C., Pereira, P., and Cuervo, A. M. (2012) Autophagy modulates dynamics of connexins at the plasma membrane in a ubiquitin-dependent manner. *Mol. Biol. Cell* **23,** 2156 –2169

53. Bejarano, E., Yuste, A., Patel, B., Stout, R. F., Jr., Spray, D. C., and Cuervo, A. M. (2014) Connexins modulate autophagosome biogenesis. *Nat. Cell Biol.* **16,** 401– 414

54. Catarino, S., Ramalho, J. S., Marques, C., Pereira, P., and Girão, H. (2011) Ubiquitin-mediated internalization of connexin43 is independent of the canonical endocytic tyrosine-sorting signal. *Biochem. J.* **437,** 255–267

55. Girão, H., Catarino, S., and Pereira, P. (2009) Eps15 interacts with ubiquitinated Cx43 and mediates its internalization. *Exp. Cell Res.* **315,** 3587–3597

56. Genoud, C., Houades, V., Kraftsik, R., Welker, E., and Giaume, C. (2015) Proximity of excitatory synapses and astroglial gap junctions in layer IV of the mouse barrel cortex. *Neuroscience* **291,** 241–249

57. Pannasch, U., Vargová, L., Reingruber, J., Ezan, P., Holcman, D., Giaume, C., Sykova, E., and Rouach, N. (2011) Astroglial networks scale synaptic activity and plasticity. *Proc. Natl. Acad. Sci. U.S.A.* **108,** 8467– 8472

58. Chever, O., Pannasch, U., Ezan, P., and Rouach, N. (2014) Astroglial connexin 43 sustains glutamatergic synaptic efficacy. *Philos. Trans. R Soc. Lond. B Biol. Sci.* **369,** 20130596

59. Tong, X., Ao, Y., Faas, G. C., Nwaobi, S. E., Xu, J., Haustein, M. D., Anderson, M. A., Mody, I., Olsen, M. L., Sofroniew, M. V., and Khakh, B. S. (2014) Astrocyte Kir4.1 ion channel deficits contribute to neuronal dysfunction in Huntington's disease model mice. *Nat. Neurosci.* **17,** 694 –703

60. Fatemi, S. H., Folsom, T. D., Reutiman, T. J., and Lee, S. (2008) Expression of astrocytic markers aquaporin 4 and connexin 43 is altered in brains of subjects with autism. *Synapse* **62,** 501–507

61. Das, A., Wallace, G. C., 4th, Holmes, C., McDowell, M. L., Smith, J. A., Marshall, J. D., Bonilha, L., Edwards, J. C., Glazier, S. S., Ray, S. K., and Banik, N. L. (2012) Hippocampal tissue of patients with refractory temporal lobe epilepsy is associated with astrocyte activation, inflammation, and altered expression of channels and receptors. *Neuroscience* **220,** 237–246

62. Schirmer, L., Srivastava, R., Kalluri, S. R., Böttinger, S., Herwerth, M., Carassiti, D., Srivastava, B., Gempt, J., Schlegel, J., Kuhlmann, T., Korn, T., Reynolds, R., and Hemmer, B. (2014) Differential loss of KIR4.1 immunoreactivity in multiple sclerosis lesions. *Ann. Neurol.* **75,** 810 – 828

63. Clarner, T., Wieczorek, N., Krauspe, B., Jansen, K., Beyer, C., and Kipp, M. (2014) Astroglial redistribution of aquaporin 4 during spongy degeneration in a Canavan disease mouse model. *J. Mol. Neurosci.* **53,** 22–30

64. Cotrina, M. L., and Nedergaard, M. (2012) Brain connexins in demyelinating diseases: therapeutic potential of glial targets. *Brain Res.* **1487,** 61– 68

65. Badaut, J., Fukuda, A. M., Jullienne, A., and Petry, K. G. (2014) Aquaporin and brain diseases. *Biochim. Biophys. Acta* **1840,** 1554 –1565

66. Abrams, C. K., and Scherer, S. S. (2012) Gap junctions in inherited human disorders of the central nervous system. *Biochim. Biophys. Acta* **1818,** 2030 –2047

67. Maezawa, I., Swanberg, S., Harvey, D., LaSalle, J. M., and Jin, L.-W. (2009) Rett syndrome astrocytes are abnormal and spread MeCP2 deficiency through gap junctions. *J. Neurosci.* **29,** 5051–5061

68. Koulakoff, A., Mei, X., Orellana, J. A., Sáez, J. C., and Giaume, C. (2012) Glial connexin expression and function in the context of Alzheimer's disease. *Biochim. Biophys. Acta* **1818,** 2048 –2057

69. Cui, Y., Masaki, K., Yamasaki, R., Imamura, S., Suzuki, S. O., Hayashi, S., Sato, S., Nagara, Y., Kawamura, M. F., and Kira, J. (2014) Extensive dysregulations of oligodendrocytic and astrocytic connexins are associated with disease progression in an amyotrophic lateral sclerosis mouse model. *J. Neuroinflammation* **11,** 42

70. Brand-Schieber, E., Werner, P., Iacobas, D. A., Iacobas, S., Beelitz, M., Lowery, S. L., Spray, D. C., and Scemes, E. (2005) Connexin43, the major gap junction protein of astrocytes, is down-regulated in inflamed white matter in an animal model of multiple sclerosis. *J. Neurosci. Res.* **80,** 798 – 808